Analytica Chimica Acta 935 (2016) 58–81

Contents lists available at ScienceDirect

Analytica Chimica Acta

journal homepage: www.elsevier.com/locate/aca

Tutorial

"Getting the best sensitivity from on-capillary fluorescence detection in capillary electrophoresis" – A tutorial

Victor A. Galievsky, Alexander S. Stasheuski, Sergey N. Krylov*

Department of Chemistry and Centre for Research on Biomolecular Interactions, York University, Toronto, Ontario M3J 1P3, Canada

HIGHLIGHTS

- Comprehensive tutorial of sensitive fluorescence detection with capillary electrophoresis.
- Critical theoretical and experimental milestones during optimization of detection efficiency.
- Graphical artworks and helpful mathematical formulas to encourage implementation of the tutorial's aim.
- Promising approaches to improvement of sensitivity in capillary electrophoresis techniques with fluorescence detection.

GRAPHICAL ABSTRACT

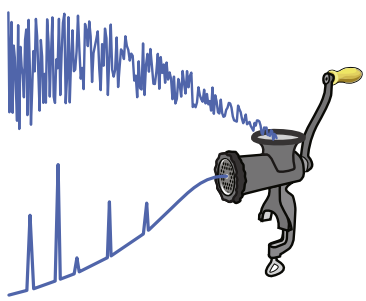

ARTICLE INFO

Article history:
Received 3 April 2016
Received in revised form
9 June 2016
Accepted 11 June 2016
Available online 20 June 2016

Keywords:
Capillary electrophoresis
Laser-induced fluorescence
Highly-sensitive detection
Optical filtration
Limit of detection
Signal-to-noise ratio

ABSTRACT

Capillary electrophoresis with Laser-Induced Fluorescence (CE-LIF) detection is being applied to new analytical problems which challenge both the power of CE separation and the sensitivity of LIF detection. On-capillary LIF detection is much more practical than post-capillary detection in a sheath-flow cell. Therefore, commercial CE instruments utilize solely on-capillary CE-LIF detection with a Limit of Detection (LOD) in the nM range, while there are multiple applications of CE-LIF that require pM or lower LODs. This tutorial analyzes all aspects of on-capillary LIF detection in CE in an attempt to identify means for improving LOD of CE-LIF with on-capillary detection. We consider principles of signal enhancement and noise reduction, as well as relevant areas of fluorophore photochemistry and fluorescent microscopy.
© 2016 Elsevier B.V. All rights reserved.

Contents

Abbreviations: ADC, analog-to-digital converter; APD, avalanche photodiode; BGE, background electrolyte; CCD, charge-coupled device; CMOS sensor, complementary metal–oxide–semiconductor sensor; FWHM, full width at half maximum; ISC, intersystem crossing; NA, numerical aperture; PMT, photomultiplier tube; RMS, root-mean-square; SMD, single-molecule detection; SNR, signal-to-noise ratio; SPAD, single-photon avalanche photodiode.

* Corresponding author.
E-mail address: skrylov@yorku.ca (S.N. Krylov).

http://dx.doi.org/10.1016/j.aca.2016.06.015
0003-2670/© 2016 Elsevier B.V. All rights reserved.

1. Fluorescence detection in CE: implementation and limitations

1.1. Introduction to CE-LIF

Separation techniques, such as electrophoresis and chromatography, are widely used in medical, biological, and chemical laboratories, because in many cases, application of the common optical spectroscopy (light absorption or fluorescence) on its own is not sufficient for reliable sample analysis. Capillary electrophoresis (CE) has clear benefits compared with different chromatographic and large-format electrophoretic (*e.g.* gel electrophoresis) methods. CE demonstrates great resolution power, flexibility, and ability to operate with a variety of different detectors, as a result providing high sensitivity in detection of analytes present at very small copy numbers of molecules.

Currently, as little as a nanoliter of the injected plug from the microliter volume of sample is sufficient for efficient CE analysis, which is a great advantage for users but which requires highly-sensitive detection for reliable analysis [1,2]. CE with Laser-Induced Fluorescence detection (CE-LIF) uses laser excitation of the fluorescent or fluorophore-labeled analytes followed by detection of emitted light (Fig. 1). After the three decades since its first reported application [3], LIF has remained the most sensitive detection approach in CE.

1.2. Beyond nanomolar concentrations

CE-LIF systems are commercially available and commonly used in analytical laboratories. Characterized by a high level of automation these instruments are designed for routine measurements with excellent robustness; however, their sensitivity is not sufficient for the accurate study of low-concentration analytes (toxins, drugs, cell metabolites, *etc.*). In some cases, researchers have to deal with small copy numbers of analyte molecules in a sample, for instance, in the analyses of contents of individual cells. For example, some molecular biomarkers may be present at as low as a single copy per cell (messenger RNAs, microRNAs, proteins, *etc.*), which corresponds to pM analyte concentrations, taking into account the volume of a typical animal cell. CE instruments cannot work with such small sample volumes; therefore, cell contents are diluted during CE-sample preparation, which further reduces the concentration of the analyte under investigation and requires the use of very advanced detection techniques. This necessitates the use of highly-sensitive custom-made setups to investigate stable ligand-target complexes with low equilibrium dissociation constant, because using commercial instruments may lead to significant overestimations of the measured constants [4]. In some cases, the copy number of analyte molecules in the sample is increased using additional amplification methods; for example, nucleic acid sequences may be pre-amplified by polymerase chain reaction, but this may introduce additional errors in the quantification procedure [5,6].

As an example of a low abundance analyte we can estimate a typical concentration of microRNAs (miRNA), which can serve as molecular markers of cancer. Fine-needle aspiration biopsy, a standard diagnostic procedure for cancer, usually yields in the order of 10^2–10^4 cells [7–10]. The total number of miRNA copies in the sample could be as few as 10^5–10^7, because typically no more than 10^3 copies of miRNA are present in each cell [11,12]. The minimum amount of studied solution is 5–10 μL to work confidently and use for multiple injections in the CE-instrument [13].

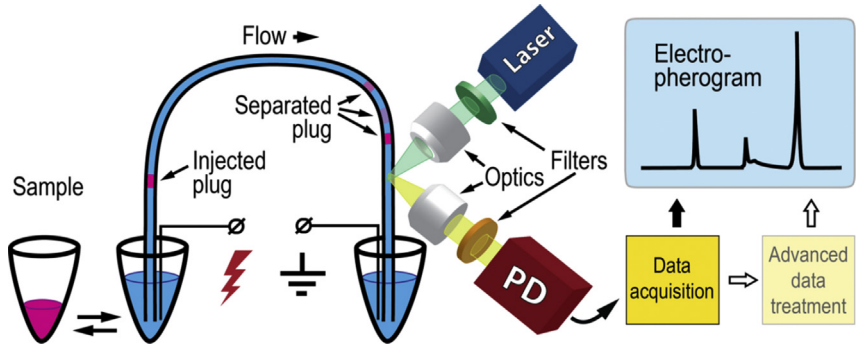

Fig. 1. Schematic of a CE-LIF setup. A small sample plug is injected into the inlet of a capillary, which is filled with a run buffer. The injected plug migrates through the capillary under the influence of an applied electric field. While moving through the capillary, different analytes separate into distinct bands due to their different electrophoretic mobilities. LIF of separated analytes passes through collimating and filtrating optics and is monitored by a photodetector. An electropherogram represents a time dependence of fluorescence intensity recorded directly from the acquisition electronics or post-processed using additional mathematical treatment of the signal.

Thus, the analyte concentration in fine-needle aspiration biopsy is about 10^{-12}–10^{-14} M.

In general, analysis of multiple analytes by CE requires injection of a short sample plug (compared to the capillary length) to allow enough room for baseline separation of multiple zones. For example, a 1.3 mm-long sample plug was used for CE analysis of 5 miRNAs in a 39 cm-long (distance to detector) capillary [14]. Due to the influence of Poisson statistics on the real number of injected analyte molecules [15], the plug must contain at least a hundred molecules, which *a priori* contributes 10% error to experimental results and yields sufficient final precision in many applications. Therefore, to gain such an amount from 10^{-12}–10^{-14} M miRNA sample with peak resolution as in Ref. [14], capillaries used should be with Internal Diameters (ID) between 13 μm and 1300 μm. We may increase the plug length four times and analyze two miRNAs instead of five, thus, decreasing the ID range to 6.5–650 μm. From the practical point of view, capillaries with ID larger than 100 μm are rarely used in CE, because only capillaries with small dimensions have high surface-to-volume ratio, which allows for the very efficient dissipation of heat generated by the electrical current in CE [13]. As a result, analytes from 10^{-12}–10^{-13} M biosamples may be reliably detected and differentiated using capillaries with ID in a range of 10–100 μm.

1.3. Optical noise in LIF detection and its reduction

With the current state-of-the-art low-noise light sources, detectors, and electronics, the optical background is the main factor limiting the sensitivity (detectability) of CE-LIF devices [16]. The predominant sources of this background is elastic (Rayleigh) and inelastic (Raman) scattering of excitation light by solvent, capillary material, and optical components. Autofluorescence of electrolyte solution and/or capillary also may contribute to the optical background. There are two developed approaches to optical detection, which exploit background suppression for the detection of weak fluorescence signals in a fluid flow and can also be used in CE-LIF instruments (Fig. 2): (i) Single-Molecule Detection (SMD) in microcapillary with internal diameter smaller than 2 μm, and (ii) post-capillary detection in a sheath-flow cuvette.

The first approach (Fig. 2a) utilizes advantages of a confined detection volume inside a microcapillary. As we mentioned above, the optical background is mainly caused by light scattering; thus, it is possible to reduce this background signal by using a small detection volume and, consequently, decreasing the amount of scattering molecules (ref. [17] and Section S1 in Supplementary Material). Confocal microscopy allows us to focus the fluorescence excitation beam to sizes close to a diffraction limit providing fL detection volumes, and this technique resulted in successful detection of single analyte molecules flowing inside microcapillaries [18–21]. This requires the use of capillaries and channels with ID smaller than 2 μm to ensure that all analyte molecules pass through the detection volume [19]. However, clogging easily happens in such extremely fine channels. As well, the large curvature of microcapillary's walls results in defocusing of the excitation beam and poor collection of fluorescence; it also promotes strong multidirectional light reflection on the glass-water interface [19]. In addition, analyte adsorption onto the capillary surface due to large surface-to-volume ratio [22,23] may increase the fluorescent background.

The second method (Fig. 2b) originates from highly-sensitive flow cytometry and exploits post-capillary detection in a sheath-flow cuvette [24]. In this cuvette, optical background reduction is based on both the contraction of the detection volume down to picoliters by hydrodynamic flow focusing, and on removing the light-reflecting glass-water interface far away from the detector field of view [25]. Another advantage of the sheath-flow cuvette is the ability to use optical-grade flat glass slabs for its fabrication, which greatly improves the efficiency of both fluorescence excitation and collection systems. Unlike SMD in microcapillary, post-capillary detection in a sheath-flow cuvette has been already adopted by CE-LIF; moreover, the best Limit of Detection (LOD) among CE-LIF setups was obtained using this technique [26–28]. However, the method has a number of inherent drawbacks. The large size of the cuvette prevents the use of high-aperture objective lenses with short working distances and reduces an efficiency of light collection. In contrast to on-capillary detection systems, sheath-flow systems make fraction collection impossible (the sample is diluted with the sheath fluid and wasted). Additionally, pre-concentration procedures, *e.g.* isotachophoresis, may require the injection of solutions at the capillary outlet [29]. In the post-capillary detection approach, the capillary outlet is inside the sheath-flow cuvette; thus, isotachophoresis followed by CE separation would be extremely difficult to perform, as it would restrict injection of both the sample and the necessary buffers to the capillary inlet. But the main drawback of this technique is the design complexity resulting in insufficient reliability for daily routine use. The alignment procedure utilizes many degrees of freedom and requires highly skilled personnel for maintenance. As a result, there is still no commercial CE-instrument utilizing post-capillary sheath-flow LIF detection method.

Direct implementation of the SMD method in CE-LIF instrument has a serious restriction regarding the finite amount of injected volume utilized in CE-LIF. SMD in microcapillary is designed for counting molecules in a continuous flow of a batch sample. It

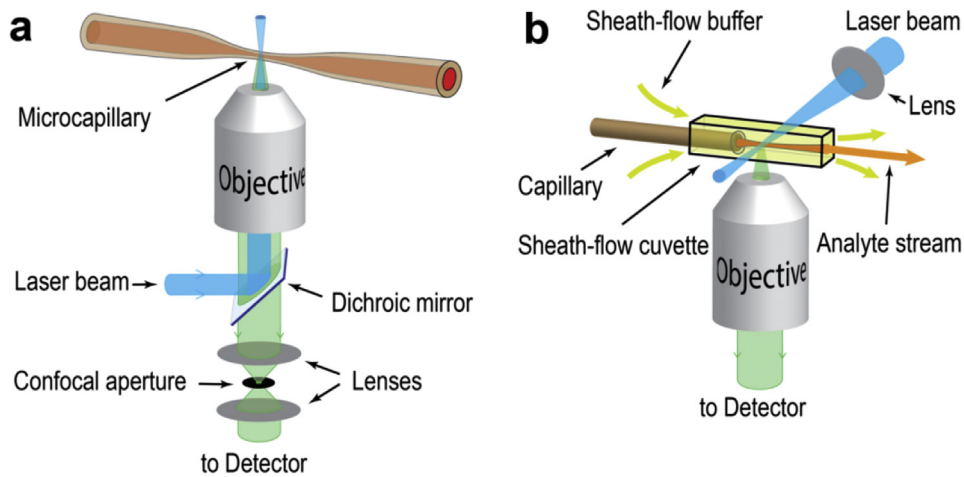

Fig. 2. Techniques available for optical background suppression: (a) single-molecule detection in a microcapillary; (b) post-capillary detection in a sheath-flow cuvette.

means that the analyte concentration can be as small as desired, because a number of analyte molecules corresponding to LOD could be "accumulated" with time from the large sample volume flowing through the capillary. In contrast, the injected volume in CE-LIF is limited and determined by the length of injected plug. The plug length is usually a few percent of the capillary length and depends on the number of separated analytes and required peak resolution [13]. The injected volume for microcapillaries ($ID < 2$ μm) is in the fL range. At least the number of molecules which corresponds to LOD must be present in the plug, making this approach less viable for rare analyte or diluted sample, e.g. molecular biomarkers.

To reach the best detectability we need to detect every analyte molecule passing through the detection window in CE–LIF, so the entire cross-section of capillary inner bore should be interrogated. The excitation/detection cylinder with diameter and length of 10 μm described in Section 1.2 will have a volume of 0.8 pL. This value contradicts with the fL-volume requirement for reliable detection of a single molecule of fluorophore in the SMD technique [18–21]. If SMD is applied to a capillary with $ID > 2$ μm, a substantial part of the analyte molecules will pass outside of the detection volume. In such a case, the fraction of detected molecules may be very small; *e.g.* a 0.1% value was obtained for a detection volume of 18 fL and capillary ID of 100 μm [30]. Such partial optical sampling is unacceptable for analysis of low-concentrated samples in analytical CE. The post-capillary detection in a sheath-flow cuvette is potentially suitable to count every analyte molecule, because the analyte stream from a large ID capillary can be focused hydrodynamically [31]. However, on-capillary detection is preferable over sheath-flow detection due to its simplicity. As a result, we need to adopt available background suppression methods, based on modern instrumentation, to obtain the best sensitivity in CE-LIF with on-capillary detection with regular capillaries.

1.4. Improvements to CE-LIF

Some special techniques may help us to detect analyte molecules from very low-concentration samples (down to fM) [32,33]. For example, a CE-LIF setup combined with wavelength-resolved multichannel detector facilitated LOD of 50 and 150 fM for sulforhodamine 101 and fluorescein, respectively [32]. This excellent detectability was obtained using a CCD camera cooled down to −125 °C by liquid nitrogen and coupled with an imaging spectrograph. The detection wavelength interval was set to collect only fluorescence light without scattering. In addition to the optimal spectral filtering, a relatively long (~2 mm) section of the capillary was observed, giving exceptional signal-to-noise ratio and LOD [32].

Castro and Shera applied a continuous-flow CE-LIF method called Single-Molecule Electrophoresis to successfully identify and detect both DNA and protein analytes using extremely diluted solutions of ~10 fM analyte concentration [33]. They employed single-molecule detection to determine the velocities of individual molecules as they migrated through two spatially separated excitation laser beams. The sample was flowing through a 100 × 100 μm square glass capillary, the diameter of each laser spots was 10 μm, while the distance between the spots was 250 μm. To gain outstanding sensitivity, analytes (DNA fragments and B-phycoerythrins) carrying multiple fluorophores were used in this work. Such an approach is not generic, as multilabeling is applicable to a limited set of large analyte molecules, whereas the B-phycoerythrin is an uncommon protein that incorporates multiple intrinsic emitters, which are equivalent to 15–20 typical organic dyes [34]. Moreover, the two-beam arrangement with 10 × 10 μm detection area led to optical sampling of only 1% of molecules flowing through the capillary detection window, and the rest 99% of sample molecules were wasted [33]. As a result, it took about 15 min of continuous detection to gain the above-mentioned ~10 fM LOD. We anticipate that a robust classical CE-LIF detection may gain an LOD comparable to nonconventional CE-LIF techniques, while simultaneously preserving the efficient separation of low-concentration samples of typical bioanalytes and providing high peak capacity (the number of species that can be analyzed in a single run).

Principles of sensitive cytometry-LIF [35] as well as CE-LIF detection [15,27,36] based on an off-capillary sheath-flow technique had been published by Dovichi and co-authors around 1990. Later, in 2004, Johnson and Landers reviewed fundamentals and practice for ultrasensitive CE-LIF detection in microanalytical systems covering both on- and off-capillary configurations [16]. In the decade after the review, new high-performance optics, lasers and photodetectors have emerged [37–40]; as well as efficient methods for in-capillary sample preconcentration [41,42] and light collection and data processing have been developed [43–46]. All of these developments, being properly applied to the on-capillary CE-LIF systems utilizing capillary with $ID \geq 10$ μm, can improve the sensitivity of ordinary instruments to a high enough level to allow work with single-cell samples, without preliminary biochemical amplification.

1.5. Outlines of the tutorial

In this tutorial, we discuss optimal excitation/detection schemes, highlight key features of optical and electronic devices, and analyze both background noise sources and methods to minimize their influence. Also we highlight some expressions and numerical values that play important roles in the process of designing and optimizing experiments.

Before delving into instrumental details (Chapters 4–6), in Chapter 2, we discuss features on an electropherogram whose quantitative characteristics can be used as Signal in CE-LIF experiments with on-capillary detection. In Chapter 3, we deduce expressions for LOD and Signal-to-Noise Ratio (SNR), which serve to compare performance of different CE instruments and configurations. Chapter 4 describes how to properly excite dye molecules under CE separation conditions, and how to improve excitation conditions to facilitate reaching the maximum SNR. In Chapter 5, we describe filtering techniques that can make extraction of useful components from the acquired signal more efficient. To properly describe the essence of spatial filtering, a specific configuration of the CE-LIF setup, a confocal one, is introduced and discussed in Chapter 5. Different types of effective detectors and detection modes are compared in Chapter 6. Selection of suitable fluorescent labels for CE-LIF is a core of Chapter 7. Two simple procedures of impurity removal from sample solutions are recommended too. In conclusion, a set of distinct steps is suggested to improve performance of an on-capillary CE-LIF setup, and future directions of CE-LIF development are outlined.

2. Definition of signal in CE-LIF with on-capillary detection

Before considering the ways to improve the sensitivity of on-capillary CE-LIF detection, we need to clarify the following concepts: i) what comprises the signal at the output of an optical detector, and ii) how the analyte properties (quantity or concentration) can be extracted from this signal.

Background signal is the detector response during a blank measurement. If the background signal is linear in time within the measurement cycle, the background signal is usually called a *baseline*. *Analytical signal* is the change in detector response due to presence of the analyte. *Total signal* is the sum of the analytical and background signals. The analytical signal is translated in to the analyte concentration by a *calibration function*.

To determine the relationship between the detected CE-LIF signal and the analyte amount, let us consider a propagation of the sample plug through the capillary. Spatial separation of analytes occurs along the capillary as they migrate under the influence of an electric field. First, let us assume that only one analyte propagates inside the capillary, and the total signal is equal to the analytical signal, *i.e.* there is no background. An excitation laser illuminates a narrow zone inside the capillary, and an optical detector measures the intensity of fluorescence as a function of electrophoretic migration time t (time passed since the start of separation) as shown in Fig. 3a, b.

When a fraction of the plug containing a fluorescent compound passes the illumination volume V_{ill}, the photodetector "observes" a luminous burst $dS^*(t)$ approximately given by Eq. (1) (see also Eqs. (S1)–(S4) in the Supplementary Material):

$$dS^*(t) \approx 2.3\alpha I_0 \phi \varepsilon V_{ill} c(t) dt, \quad (1)$$

where α is the collection efficiency of the optical scheme, I_0 is the intensity (power density) of excitation light, dt is the residence time of analyte in the illumination volume, ϕ and ε are the fluorescence quantum yield and the molar absorption coefficient of the fluorescent analyte, respectively, $c(t)$ is the average concentration of the analyte in the illuminated volume V_{ill}.

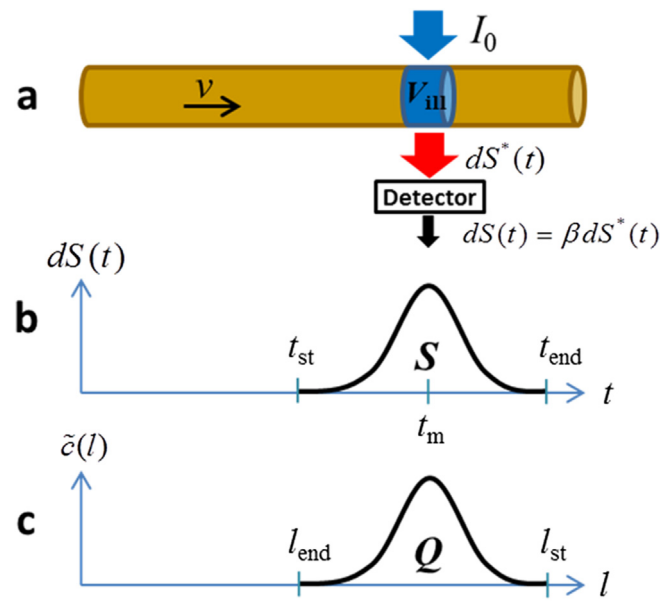

Fig. 3. (a) Schematic of the CE-LIF detection, where V_{ill} is a volume illuminated by light with intensity I; $dS^*(t)$ and $dS(t)$ are fluorescence intensity and electrical signal at the detector output, respectively, and v is a velocity of analyte zone. (b) Plot of the detector signal $dS(t)$ as a function of electrophoretic migration time t. S is the integrated signal in a time range between t_{st} and t_{end}. (c) Distribution of the analyte concentration $\tilde{c}(l)$ along the capillary at time t_m. Q is analyte amount in the sample plug with boundaries l_{st} and l_{end}.

Eq. (1) is valid if V_{ill} is fully observed in the field of view of the light-collecting optical system; otherwise, it is necessary to calculate the overlap between the illuminated and observation volumes and use the calculated value in Eq. (1). We called this overlap "detection volume", and Section 5.1 contains the description of possible mutual arrangement of illuminated and observation volumes. As V_{ill} is small, the optical density of the analyte along the excitation beam is also minor. Such small-scale CE geometry is advantageous for optical detection in a wide range of analyte concentrations, as it allows uniform excitation along the laser beam and reduces effects of fluorescence reabsorption and self-quenching. The fluorescence signal $dS^*(t)$ is transduced into electrical signal $dS(t)$ by the photodetector and acquisition electronics with a conversion factor β ($dS(t) = \beta dS^*(t)$). Acquired signal $dS(t)$ corresponds to the local analyte concentration in the flow volume that is visible through the detection window at a time t. Area S represents a time integral from signal start (t_{st}) to signal end (t_{end}):

$$S = \int_{t_{st}}^{t_{end}} \beta dS^* = 2.3\alpha\beta I_0 V_{ill} \phi \varepsilon \int_{t_{st}}^{t_{end}} c(t) dt \quad (2)$$

As a result, the total acquired signal S is a function of integrated analyte concentration, but in a general case the concentration itself is not an additive parameter. To integrate quantities instead of concentrations, we must transform the time integral into a spatial integral using substitution $t = l/v$, where l is the distance along the capillary and v is the velocity of analyte zone. By using the distribution of analyte concentration along the capillary, $\tilde{c}(l)$ and positions of plug start and end, l_{st} and l_{end}, respectively (Fig. 3c), we obtain:

$$S = 2.3\alpha\beta I_0 V_{\mathrm{ill}}\phi\varepsilon \int_{l_{\mathrm{st}}}^{l_{\mathrm{end}}} \frac{1}{v}\tilde{c}(l)dl \quad (3)$$

The velocity of analyte zone v is constant and can be calculated from the migration time t_{m} of analyte peak apex: $v = L_{\mathrm{det}}/t_{\mathrm{m}}$, where L_{det} is the distance from the capillary inlet to the detection window. Using substitution $\gamma = L_{\mathrm{det}}/(2.3\alpha\beta I_0 V_{\mathrm{ill}}\phi\varepsilon)$, we get an expression for the total analyte quantity Q inside the capillary:

$$Q = \int_{l_{\mathrm{st}}}^{l_{\mathrm{end}}} \tilde{c}(l)dl = \gamma\frac{S}{t_{\mathrm{m}}} = \gamma E_{\mathrm{S}} \quad (4)$$

The value $E_{\mathrm{S}} = S/t_{\mathrm{m}}$ is a corrected peak area which is strictly proportional to the analyte quantity Q according to Eq. (4) in the assumption that the analyte parameters ϕ and ε are constant. Also we postulate that all analyte molecules defining the peak have the same migration time t_{m}. *Consequently, the corrected peak area* E_{S} *should be used as an analytical signal in quantitative* CE-LIF *with on-capillary detection.* This necessity arises due to slower molecules residing in the illumination/detection volume for a longer time, thus having more chances to absorb and then to emit light. Consequently, peak widths for analytes with different mobilities are inversely proportional to their velocities. Note, that for the post-capillary detection in the sheath-flow systems the velocities of analytes are defined mainly by the accelerated flowrate of the hydrodynamically narrowed stream, and the correction of the peak area by the migration time is not needed.

Signal intensity of an on-capillary optical detector (including both absorbance and fluorescence detectors) at any given time is proportional to the analyte amount in the detection volume at that time (see Eq. (1)). In other words, the detector monitors the average concentration of analyte molecules in the capillary in a detector position. Such type of a detector is usually called a *concentration-sensitive* detector. Another type of detectors, named *mass-sensitive*, counts the number of analyte molecules that flow through the capillary cross-section per time unit. An example of such a detector is ESI-MS detector that measures a flux of the analyte. Note, that the post-capillary optical detection in the sheath-flow systems also belongs to the class of *mass-sensitive* detectors (see Section S3 in Supplementary Material for details).

There is a simple rule to distinguish these two types of detectors. If we stop the flow in the capillary, the *concentration-sensitive* detector will show a constant signal, whereas the signal in the *mass-sensitive* detector will fall to the background. Time-resolved signals measured by any *concentration-sensitive* detector require a peak area correction for the peak migration time; because the concentration is not an additive value along the time coordinate. In *mass-sensitive* detectors, the correction of the peak area by the migration time is not needed.

In contrast to the above-considered no-background assumption we usually observe a non-zero baseline in CE experiments. In this case, the analytical signal E_S is defined as peak area above the mean baseline level divided by the migration time t_{m} of the peak apex (Fig. 4).

Unlike the peak width, the peak height is not affected by the analyte velocity and is frequently used in CE as the analytical signal instead of the corrected area. The peak height is measured from the baseline to the peak apex. The substitution of the area with the peak height is valid only if the peak shape does not change significantly with changing analyte concentration. Therefore, a researcher should be very careful with using the peak heights instead of areas, as a variety of factors can distort peak shape, for example, (i) stacking/destacking due to an unmatched ionic strengths of the sample and run buffer or (ii) the electrodispersive effect due to high sample concentrations [47]. In the range of moderate and high analyte concentrations, a nonlinear calibration function can be utilized to take advantage of peak height for quantitative analysis.

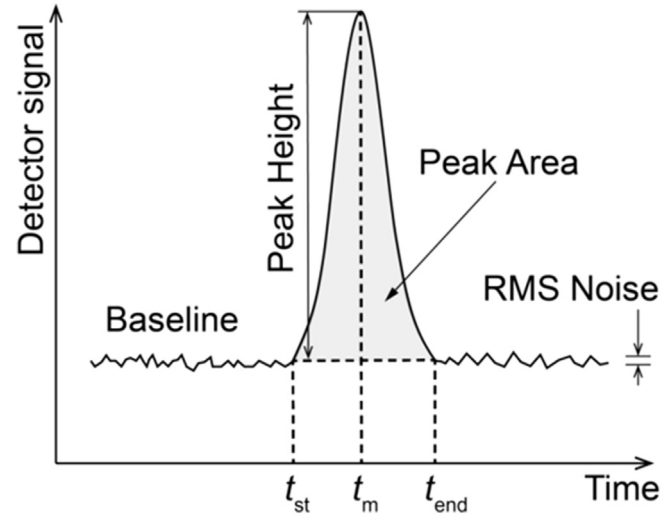

Fig. 4. Determination of an analytical signal from the electropherogram with non-zero baseline. t_{m} is a migration time of the peak apex, t_{st} and t_{end} are time boundaries of the peak.

While working with a small number of molecules in the sample we must remember that the statistical accuracy of the measured properties becomes low. The analyte molecules are not uniformly distributed within very dilute solutions, and their quantity in the injected plug is governed by the Poisson statistics. This non-uniformity leads to a plug-to-plug variation in the number of sampled analyte molecules, which is called the molecular shot noise [15]. The standard deviation of the peak area produced by the molecular shot noise is inversely proportional to the square root of the number of injected analyte molecules. For example, at least 10^4 analyte molecules are required to get a relative precision of 1% for the number of injected molecules and for other parameters linked to this number (peak area, *etc.*) [15]. The final error for the measured number of the injected molecules will be higher than that caused by the molecular shot noise as this noise is only one of many different sources of error in such experiments.

Another problem associated with small numbers of analyte molecules in the sample arises under extremely low analyte concentrations. The measured signal no longer appears as a continuous peak but breaks up into a series of spikes, corresponding to fluorescence bursts of individual analyte molecules, and the signal treatment has to be turned to the SMD mode (Fig. 5).

In the SMD mode, there is no continuous signal anymore, we have a series of individual spikes, and, thus, specific data treatment methods, based on counting fluorescence bursts, should be utilized in analyzing single-molecule signals [48,49]. Multiple photon bursts can be produced by a single fluorophore molecule, when it is excited cyclically in the intensive laser beam with a time period defined by fluorescence lifetime. SMD universally uses photon-counting technique, in which the burst size is defined as the number of detected fluorescence photons pertaining to single molecule. Burst examination provides more information about the analyte than a simple quantity determination by counting molecules. The burst length corresponds to the residence time in the detection volume that is specified by the analyte velocity, whereas

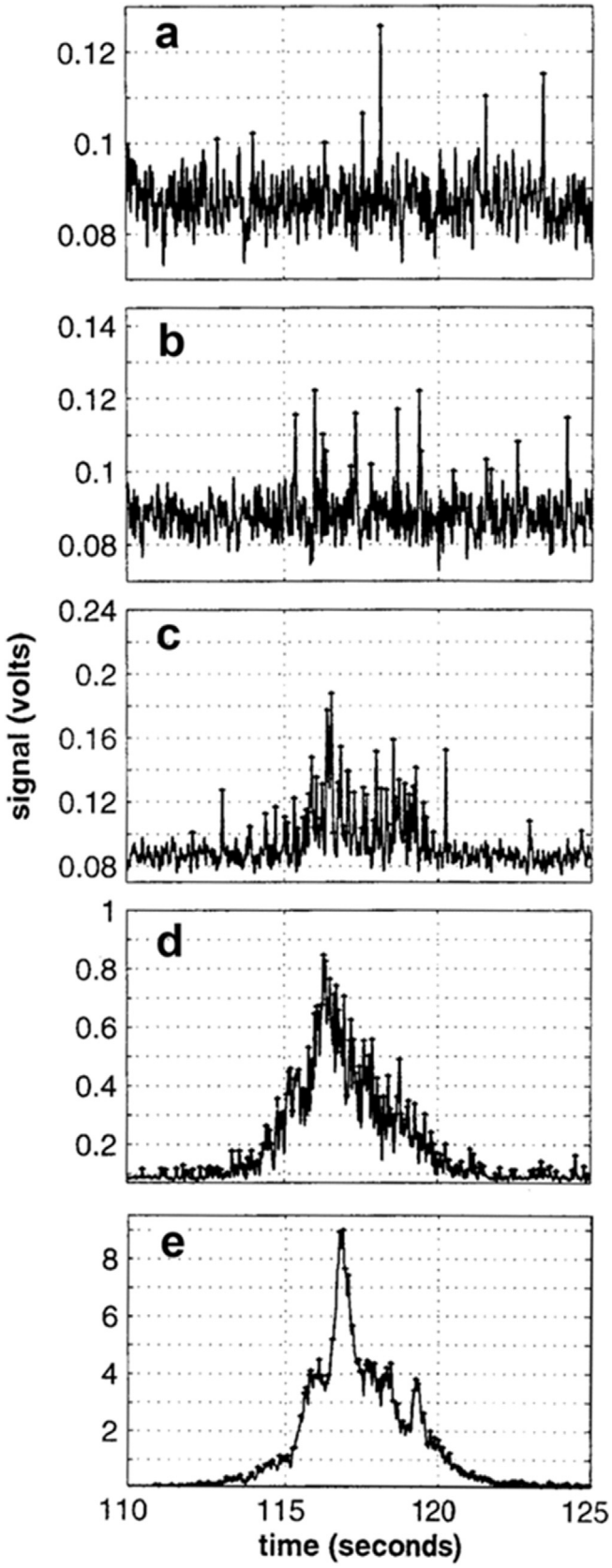

Fig. 5. Repeated injection of different quantities of B-phycoerythrin. Only the part of the electropherogram that represents analyte peaks is shown. Injected plug contains: (a) 15 molecules; (b) 30 molecules; (c) 300 molecules; (d) 3000 molecules; (e) 30,000 molecules. Adapted with permission from Ref. [15]. Copyright© 1996 American Chemical Society.

the burst size is defined by the fluorophore's photophysical properties (molar absorption coefficient, quantum yield, and fluorescence spectrum). Statistical analysis of both the temporal intensity fluctuations (such analysis is named Fluorescence Correlation Spectroscopy) and the burst size distribution are successfully used for determination of the photophysics and dynamics of individual molecules by the SMD technique [50,51]. These advanced methods of data treatment allow identification of different fluorophores in flow and have great potential in resolving multiple analytes in a single CE-LIF run. Because of the necessity to use expensive equipment with complex data treatment as well as the need for a highly-trained operator, such SMD approach is still not used in analytical CE. Therefore, in this tutorial, we will not consider the peculiarities of obtaining and analyzing signals in the SMD mode.

A classical approach to treat the SMD data may be still employed, as in the case shown in Fig. 5. Using a known plug width, which is determined from the additional calibrating measurements (Fig. 5e), single-molecule bursts corresponding to one of the analytes in the plug (Fig. 5a) can be integrated into a single peak with the total area roughly proportional to the analyte quantity Q. As a result, the SMD data may be analyzed as a classical electropherogram, where a single peak corresponds to a single analyte.

3. Limit of detection and signal-to-noise ratio

To discuss and compare CE instruments in the context of analyte detectability, at first we need to consider suitable quantitative characteristics. The relevant parameters of merit include limit of detection (LOD), sensitivity, linear dynamic range, and limit of quantitation (LOQ).

Limit of detection (LOD) is defined as the lowest concentration of an analyte present in a sample that can be differentiated from the background noise with a specified level of confidence. LOD is a critical figure of merit since a CE technique cannot yield a valid result if the concentration or amount of analyte in the measured sample is below LOD. *Sensitivity* describes the ability of an instrument to distinguish different amounts of analyte. According to IUPAC definition the sensitivity is equal to the gradient of the calibration curve (plot of signal versus amount of analyte) [52]. *Linear dynamic range* is a range of concentrations over which the calibration curve is linear and the slope m (*i.e.* sensitivity) is constant (Fig. 6).

In mathematical terms, LOD is the analyte concentration that produces an analytical signal E_S equal to $k\sigma_{bk}$, where k is a confidence factor, σ_{bk} is a standard deviation (SD) of the blank measurement E_{bk}. The factor k is usually equal to 3 and, thus, LOD is typically defined as:

$$LOD = \frac{3\sigma_{bk}}{m} \tag{5}$$

A mean analytical signal at the LOD is slightly above the variability of the blank measurement so it represents concentration that can be detected but not necessarily quantitated. The larger the specified value of k, the more likely it is that the determined signal is caused by the analyte and not by a random error. The lowest concentration of an analyte in a sample that can be quantitated with suitable precision and accuracy is named *limit of quantification* (LOQ). The value of $k = 10$ is usually used as a rule of thumb for a definition of LOQ:

$$LOQ = \frac{10\sigma_{bk}}{m} \tag{6}$$

LOD can be improved by decreasing of σ_{bk} for a given slope m or by increasing the slope value for a given σ_{bk}. The term "better

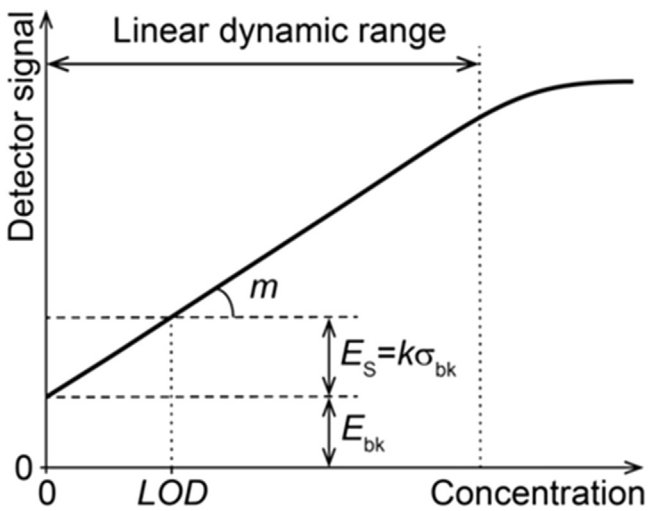

Fig. 6. Concentration calibration curve and graphical interpretation of LOD.

detectability" characterizes the detection behavior of the instrument in the former case whereas the term "better sensitivity" is preferable for using in the latter case. In the current tutorial, we usually utilize the term "highly-sensitive detection" when we describe the ability of the instrument to measure low concentrations of analyte without specifying how it was achieved. In the other words, we associate "highly-sensitive detection" with lower values of LOD and LOQ.

To determine LOD and LOQ through the Eqs. (5) and (6) the slope m is calculated from the plot of corrected area versus the analyte concentration in the injected plug. The value of σ_{bk} is determined as SD of blank injections and, according to the IUPAC guideline [52], σ_{bk} should be based on at least 6 independent blank measurements. In CE with LIF detection this approach to measurement is not convenient in practise, because the signal of a blank injection is difficult to identify. Signal of sample buffer, used usually in blank measurements, does not exceed the average fluorescence background signal and boundaries of the blank peak are indeterminate. In this case, the procedure based on the linear regression analysis of the calibration curve in the low concentration range should be utilized for the correct σ_{bk} determination. Residual SD of the regression line or SD of y-intercepts of regression lines may be used for the LOD calculation in such a case [53]. These calibration-curve-based procedures of LOD determination are complicated and time consuming, and are rarely applied to CE-LIF measurements.

In the CE-LIF method, SD of the blank injection is limited by the noise N in the fluorescence background ($E_S = \sigma_S = 0$, $\sigma_{bk} = N$, $E_{bk} = E_B$); therefore, an alternative approach to LOD estimation, based on signal-to-noise ratio (SNR), is widely used. In the SNR, signal is defined as the analytical signal E_S; whereas the noise is SD of the background signal, also called root-mean-square (RMS) noise. At the concentration of analyte near LOD the SNR is equal to the confidence factor k:

$$SNR = E_S/N = k\sigma_{bk}/\sigma_{bk} = k \tag{7}$$

Such option of LOD estimation is implemented according to the ICH Guideline: "Determination of SNR is performed by comparing measured signals from samples with known low concentrations of analyte with those of blank samples and establishing the minimum concentration at which the analyte can be reliably detected" [53].

To assess the detection limit of an instrument, the measurement of the peak height as analytical signal is generally accepted due to negligible distortion of peak shape at low concentrations. Moreover, peak height may be preferable when SNR is poor and the starting and ending boundaries of a peak are determined with a large error.

A classical method of LOD estimation developed by Knoll for chromatographic data [54] uses the peak-to-peak value of baseline noise in fixed intervals before and after the peak, instead of the RMS noise, for simplicity of manual calculations. With the advent of modern computerized data analysis methods it is no longer difficult to calculate SD of the background signal over a selected region of the electropherogram baseline.

For a single CE-measurement $SNR = E_S/N$, where E_S is the peak height and N is the RMS noise derived from n data points on the baseline according to:

$$N = \sqrt{\frac{\sum_{i=1}^{n}\left(E_{B,i} - \overline{E_B}\right)^2}{n-1}} \tag{8}$$

The value of analytical signal E_S usually varies from measurement to measurement. Multiple CE experiments (at least 6 [52]) are necessary to determine the total variance σ_S^2 of the analytical signal that includes, besides the variance of the noise of detection system, variances of: the injected amount; the amount of sample transferred through the capillary; the amount of contaminants in the background electrolyte (BGE); and the excitation power. The average SNR obtained from repetitive CE measurements of a single sample is usually accepted for the LOD estimation. Nevertheless, the single-sample approach does not capture the sample-to-sample variation, and repeated measurements of different samples are highly recommended.

Standard deviation σ_S of the analytical signal for multiple CE experiments is determined using the following expression:

$$\sigma_S = \sqrt{\frac{\sum_{i=1}^{p}\left(E_{S,i} - \overline{E_S}\right)^2}{p-1}} \tag{9}$$

where p is a number of independent CE measurements The total measured signal equals $E_S + E_B$ (Fig. 6); so the noise in the total signal is due to the sum of the noise contributions from the analytical signal σ_S and the baseline N. Finally, we have the following expression for calculation of SNR in case of multiple CE measurements:

$$SNR = \frac{\overline{E_S}}{\sqrt{(\sigma_S^2 + N^2)}} \tag{10}$$

A simple strategy of getting the lowest value of LOD in CE-LIF detection is to improve SNR. As we see from Eq. (10) it can be done by increasing the signal (E_S) and/or decreasing the noise $(\sigma_S^2 + N^2)^{0.5}$. The direct method of signal gain, due to increasing laser light intensity, has serious limitations and will be discussed in Chapter 4. The optimization of noise level is a more sophisticated process and requires the knowledge of the dominant noise sources in a given experimental setup. Noise sources, SNR expressions for the fluorescence detection and strategy for the SNR optimization are discussed in Chapters 5 and 6.

4. Excitation

The first combination of CE with LIF was used to separate and detect a number of derivatized amino acids [3]. Subsequent advances in laser manufacturing and development of reliable semiconductor lasers have resulted in the fast progress of the CE-LIF technique [2,55,56]. A laser beam may be readily delivered and

focused in capillaries of micrometer-range diameters resulting in high optical power density and efficient excitation of any fluorescent molecules passing the capillary. As we showed in the Chapter 3, an increased number of excited fluorescent molecules leads to an improved SNR, but two factors limit the excitation efficiency: possible photodamage of the dye molecule and its non-ideal photophysics.

4.1. Photostability of fluorophore

In order to describe the photostability issue, we consider an example when the illuminated volume contains *a single* molecule of fluorescein during the time interval necessary for this molecule to pass through the illuminated volume (Fig. 3a). For capillary ID and laser beam waist of 10 μm we may approximate this volume as the volume of a sphere with a 10 μm diameter, thus, a single analyte molecule will result in ~3 pM concentration. If the excitation power is 1 mW for 488 nm of continuous laser, then the power density, I_0, will be 1.27 kW cm^{-2} or 3.11×10^{21} photons cm^{-2}/s. The absorption cross-section of fluorescein, θ, is 3.06×10^{-16} cm^2 for 488 nm light [57]. As a result, each ground-state molecule is excited with a rate constant of $\theta I_0 = 9.5 \times 10^5$ s^{-1}. A typical migration velocity in CE is on the order of 1 mm/s [14,58,59]; thus, one fluorescein molecule passes through the 10 μm excitation spot in ~10 ms, which gives ~10^4 excitation events per molecule and substantially increases SNR in comparison with the case when one molecule emits only one photon being in detection volume. But, under such experimental conditions, fluorescein molecules are brought nearly to their photodegradation threshold, due to increased probability of photoreaction after multiple excitation-relaxation cycles [60,61]. Therefore, excitation conditions should be chosen in accordance with the photostability of the employed dye. For example, if we increase the capillary ID and the laser beam waist by a factor of 5 (to 50 μm), then the travel time of fluorescein through the detection volume will become 5 times longer, but power density will be 25 times lower. The resultant number of excitation events will become ~2×10^3, which is ~5 times lower than the photodegradation limit of fluorescein, and such excitation conditions prevent appearance of possible artifacts due to dye photodecomposition.

In typical electrophoretic separation, the analyte plug migrates at a certain average velocity, which depends on the electric field and the electrophoretic mobility of molecules of interest. Obviously, under the constant excitation intensity, the rate of photodamage depends on the analyte's migration velocity. In most cases, it is easier to change the excitation energy than the migration velocity; thus, the optimal excitation energy should be determined at a given velocity.

4.2. Saturation effect

Photophysical properties (*e.g.* lifetime and quantum yield) of fluorophore molecules should also be taken into account when maximizing SNR. In order to demonstrate this effect, let us imagine that two or more molecules pass a 10 μm illuminated volume under intense excitation. In this case, while increasing the laser intensity, it should be possible to excite a large part of the fluorophore molecules and reach the saturation limit in absorption/emission, while any further increase in the excitation intensity will provide negligible increase in the number of emitted photons. This parameter (the saturation limit) may be characterized using the population ratio, r, between the number of molecules in the excited state to the total number of molecules in the illuminated volume (Eq. (S9) in Supplementary Material):

$$r = \frac{\theta I_0 \phi_f}{k_f + \theta I_0 \phi_f} \tag{11}$$

where θ is an absorption cross-section of the studied molecule, I_0 is continuous excitation intensity, ϕ_f is fluorescence quantum yield, and k_f is a radiative rate constant for molecules in the excited singlet state.

Eq. (11) provides population ratio r in ideal two-level systems (ground state plus 1st excited state) without any background signals. If the product $\Theta I_0 \phi_f$ is much greater than the value of k_f, then r will approach unity (saturation limit). The opposite case ($\Theta I_0 \phi_f \ll k_f$) is the condition of non-saturation intensity of excitation. For fluorescein ($k_f \sim 2.2 \times 10^8$ s^{-1}, $\phi_f \sim 0.9$ [62]) passing a 10 μm sphere (~7.9×10^{-7} cm^2 cross section) of the 488 nm line, the laser density should be much less than $k_f/(\Theta\phi_f) = 0.33$ MW/cm^2, corresponding to a power of 0.26 W. Still, non-saturation intensity may introduce non-linearity during the measurements due to photodamage in some types of dyes. For example 1 mW power beam may be treated as non-saturation according to Eq. (11), though it may cause photo-damage of fluorescein samples (see Section 4.1 about the photostability issue).

Fluorescein is known to undergo intersystem crossing (ISC) or, in other words, have a non-zero yield into the triplet state ($\phi_{ISC} = 0.03$ [57,63]) which is more long-living than the singlet state (~1 μs *vs.* 4.5 ns [57]) and leads to the necessity of considering a three-level system. Under the steady-state excitation we may derive the following expression for the ratio between the number of molecules in the excited state to the total number of molecules in the illuminated volume (Eq. (S27) in Supplementary Material):

$$r = \left[1 + \frac{k_f}{\phi_f}\left(\frac{\phi_{ISC}}{k_T} + \frac{1}{\theta I_0}\right)\right]^{-1}, \tag{12}$$

where k_T is a rate constant of fluorophore relaxation from the triplet state, ϕ_{ISC} is the quantum yield of intersystem crossing.

Applying Eq. (12) we can predict how many molecules will produce useful signal when they emit from the excited singlet state. Most of fluorescein molecules (~97%) will stay in the ground state and less than 1% will occupy the excited singlet state in a beam waist of 10 μm at a 1 mW laser power (Table 1). Theoretically, 100 mW power will result in onset of saturation for the 1st excited singlet state of fluorescein. The above-presented evaluations do not take into account scattering, reflection, absorption by impurities and other loses of excitation light (see Section 4.3), but can act as a starting point to find optimal excitation power and power density.

4.3. Optimization of excitation conditions

As briefly mentioned in the introduction, Raman and Rayleigh scattering, as well as autofluorescence of BGE and/or capillary, are the main sources of the background signal for modern electrophoretic systems. Scattering is directly proportional to the used optical power density of excitation light. Autofluorescence deviates from linear dependency on power density slower than fluorescence of typical fluorophores. Therefore, the total background signal has only slightly nonlinear dependence on the laser power density under typical excitation condition in CE-LIF [16]. As a result, there is an optimum range of excitation energies which gives the maximum value of *SNR*, avoiding severe photodegradation, saturation, and others artifacts (Fig. 7). For example, Mazouchi et al. successfully used a similar approach to find optimum excitation power (Fig. S3 in Ref. [64]) in CE-LIF measurements.

Obtaining high excitation power is not a problem with laser

Table 1
Population of ground, 1st excited singlet, and 1st excited triplet states under different excitation conditions.

Laser power, mW	Population of different states		
	Ground state	1st excited singlet state	1st excited triplet state
1	97%	0.4%	2.6%
10	75%	3%	22%
100	23%	10%	67%
1000	3%	13%	84%

sources. Lasers typically used in CE-LIF applications generate light beams with near Gaussian intensity profiles. Such beams can easily be focused into a small volume (down to a diffraction-limited spot, see Section 5.1.1) and allow us to get a very high light intensity in the focus. Sometimes multimode optical fibers are used for laser-light delivery; however, such type of waveguides should be used with caution in highly-sensitive setups because they decrease the quality of the Gaussian-beam profile (see next Section 4.4).

Round capillaries are widely used for their practical convenience. However, the cylindrical walls of such capillaries act as astigmatic lens. The influence of the wall curvature is especially strong when the lens with a high-numerical aperture is used to deliver/collect light to/from the capillary. In this case, the focused Gaussian laser beam does not have a circular cross-section inside the capillary cavity, as shown in Fig. 8a. The illuminated volume is enlarged significantly, the laser power density drops down, detection optics also capture fluorescence and background signal from the larger detection volume, and SNR is accordingly lower [19]. To overcome such obstacles Lundqvist et al. studied a set of capillaries of different diameters (curvature) and wall thicknesses [20]. They found the optimum capillary dimensions (150 μm outer diameter, 30 μm ID) resulting in the maximum SNR under the condition of fixed excitation power, which should be preliminary estimated as non-destructive and non-saturating for the studied dye.

The light beam distortion caused by cylindrical capillary walls may be minimized by using an immersion objective lens with an immersion liquid (silicone oil or glycerol) which has a refractive index matching the refractive indices of the capillary wall and the sample solution (Fig. 8b). This seems to be a very promising way to get fine focusing of light beams inside round capillaries and to reach the highest values of SNR. Another approach to improving light focusing in CE-LIF is by using a capillary with a square cross section [65]. An additional advantage of square capillaries is the possibility to relatively easily predict the trajectories of excitation and fluorescence beams due to the flat surface of capillary wall. But separation efficiency may be reduced in square capillaries in comparison with the round ones as was found by Xu et al. [65]. Also, to obtain reproducible results the square capillaries require additional pre-alignment in CE-LIF instruments with exchangeable capillary holders (cartridges), making the setup less user-friendly and robust.

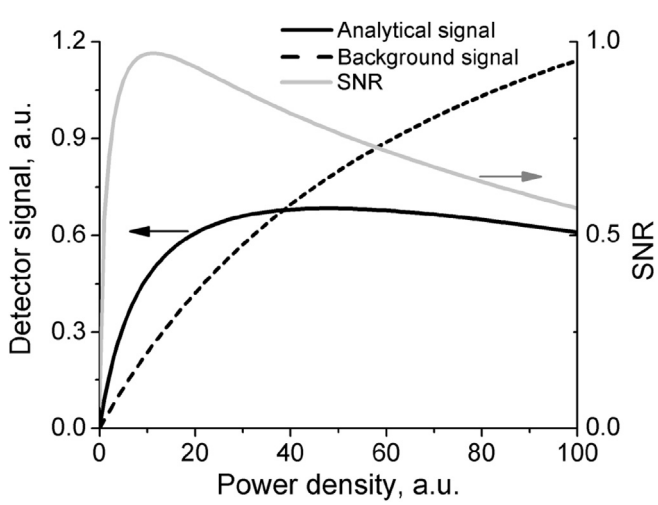

Fig. 7. Simulated analytical signal (solid) and background signal (dashed), as well as SNR (grey) are plotted as functions of optical power density of incident light. SD of background signal is calculated as square root of background intensity under the assumption of Poisson photon counting statistics.

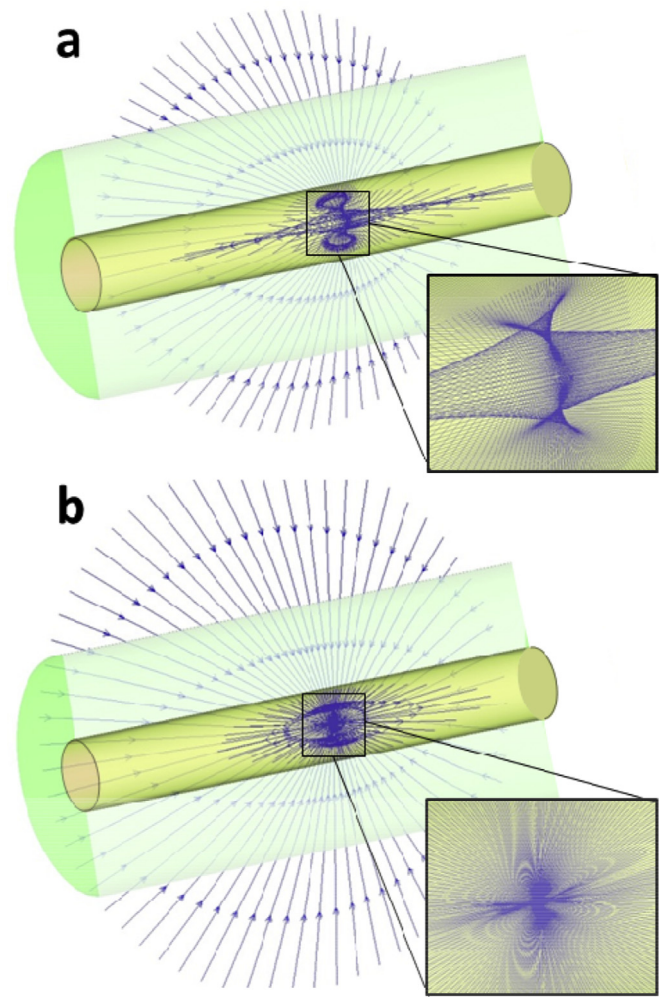

Fig. 8. Ray-tracing simulation of monochromatic light beam focused into a silica capillary (with a refractive index $n = 1.46$) using two types of objective lenses (60×, NA 1.3): (a) a lens with ordinary immersion oil ($n = 1.52$), and (b) a lens with silicone immersion oil ($n = 1.41$). The capillary has external and internal diameters of 66 and 20 μm, respectively, immersed in oil, and filled with water ($n = 1.33$). For simplicity only marginal rays, capillary cavity, and a half of the capillary wall are shown. The ray-tracing simulation was made by Zemax (Kirkland, WA) with a lens design based on Olympus patents [66,67].

4.4. Excitation sources and light delivery

Lasers generate light beams of high optical quality, which implies that such beams may be focused into tiny spots close to diffraction limit. Such beams, while collimated, will also maintain small profile over greater distances. The beam quality is closely related to such parameters as level of spatial coherence and beam profile (*e.g.* Gaussian beam). Most modern lasers generate near-Gaussian beams, and their comparison with ideal Gaussian profile serves as a measure of laser quality shown in laser test-sheets. As a result, such lasers provide high power density in focused beam-waist and make it possible to further miniaturize analytical devices.

A CE review with a detailed description of available excitation sources was published more than 10 years ago [68]. Since that time, semiconductor lasers progressed substantially and substituted many different types of lasers in a great number of applications including CE-LIF [55,56]. Technologically, semiconductor laser chips emit laser beams of rectangular cross-section. At the same time, such cross-section may be readily transformed by special optics into a round one. For example, coupling semiconductor laser with a single mode fiber results in a Gaussian-shaped beam.

Optical waveguides are very convenient for delivery of the excitation beam over relatively long distances to any point in the fluorescence setup. They also allow switching the excitation source without additional rearrangement of the optical scheme. Single-mode fiber is a special type of waveguides, as an output beam after single-mode fiber always has a Gaussian shape. Disadvantageously, these waveguides have core diameters not exceeding several microns; their numerical aperture (NA) is of the order of 0.1, which requires additional optical components to input laser light efficiently into the fiber core, though near-twofold loss of laser energy is unavoidable [39,69]. Multi-mode waveguides have larger numerical aperture, and may have a relatively large core diameter of up-to hundreds of microns. Thus, it is easier to input laser light into such waveguides, with no need for expensive optics and mechanics; however, their use does change the output beam profile from the desired Gaussian shape. As a result, diode lasers with multimode waveguides are only suitable for applications which do not need tiny excitation beam spots.

The size of a focal spot can be estimated by means the *optical invariant* $NA \times y$. This product of numerical aperture NA and an object linear size y is a constant throughout the optical system. In our case, we need to find an image of the fiber-core end focussed by the objective lens into capillary hollow. Usually multimode fibers having a core diameter of 100–200 μm and $NA = 0.22$ are used for laser coupling in CE-LIF. A light beam exiting from the fiber of 200 μm ($NA \times y$ ~44 μm) will be focussed to the spot of 55 μm diameter by an objective lens with $NA = 0.8$ (maximal NA value for non-immersion lenses). Such a spot size is suitable for most CE-LIF applications except SMD and highly-sensitive instruments, where very tight focusing is required for excitation beam.

Recently, Light Emitting Diodes (LEDs) have become a viable alternative to lasers for luminescence measurements, including the field of CE [70]. Currently, on-capillary LED-based CE-devices provide nanomolar and subnanomolar LOD values for fluorescein and riboflavin [71–75], which are still worse than (although quite close to) LOD characteristics of optimized systems with laser excitation and confocal detection [59]. The two following paragraphs uncover the reasons for this difference in LOD.

Position of central wavelength of excitation band determines both the intensity of fluorophore fluorescence and the spectral profile (intensity *vs* position) of spurious signal consisting of scattered light and background luminescence. Typical UV–vis LEDs have a band with a full width at half maximum (FWHM) of 10–30 nm [76], which is much greater than a typical 3 nm FWHM of a diode lasers' band [77]. Wider excitation band causes wider band of elastically and non-elastically scattered light. Therefore, it is difficult to properly filter the fluorophore luminescence from the scattered light and, thus, to gain the maximum possible SNR. Moreover, a typical LED emission spectrum incorporates a long-wavelength tail which extends up-to the detection region of fluorophore luminescence [76]. High-quality band-pass filters may help to narrow LED emission spectrum, though the excitation power would be reduced by several folds.

LEDs and lasers demonstrate comparable power of radiation, but LED emission is extremely hard to focus tightly while maintaining sufficiently high optical power. Power LEDs have emitter size of more than 1 × 1 mm, and they are usually coupled with optical waveguides for light delivery in the CE-LIF applications. Let us consider the same multimode fiber with $NA = 0.22$ and a core of 200 μm, as in example above, to create a suitable focussed spot of a 55 μm diameter. The optical losses are about 100–200 times for an LED coupled to such multimode 200 μm fiber [76,78]. We can see that only an insignificant fraction of the light emitted by the LED is used for fluorescence excitation. As a result, in order to obtain as much fluorescence light as possible by means of multiple excitation-relaxation cycles, microfluidic setups are recommended to be equipped with lasers rather than LEDs until the next generation of very powerful and reliable LEDs becomes commercially available. After that, robustness and low cost of the powerful LED will make such light sources very attractive for use in the CE-LIF instruments.

5. Filtration

Filtration attenuates some unwanted signal components and helps to collect useful signal. The use of filtering reduces random errors and increases the SNR due to a reduction of the background signal magnitude and, thus, background noise. The fluorescence emission in CE-LIF may be characterized by the following parameters: intensity, wavelength, lifetime, polarization, and spatial location. Intensity filtering is the most conventional method to discriminate the analyte signals from the background. Additionally, spatial, spectral, temporal, and polarization features of emitted light can be used for the optical filtering.

5.1. Spatial filtering

The collecting optics in CE-LIF should detect only molecules flowing inside the capillary, whereas the capillary walls and other optical elements on the optical pathway, which are potential sources of background, must not be captured in the detection volume. Here and further the detection volume means illuminated volume in the field of view of detection system (Fig. 9). For spatial filtering, high-resolution optics is needed to accurately focus the excitation light and collect fluorescence from the confined space.

5.1.1. Objective lens

The objective lens is a key component of the optical system, which allows us to manipulate the light beam. The smallest size of the point in which the objective lens is able to focus light is determined by the lens design (lens compensation of optical aberrations), by the intensity profile of the light beam (Gaussian laser beam or uniform illumination), and by the diffraction limit related to the wave nature of light. The minimal beam waist at the focal plane for aberration-free optics is given by the following expression (Fig. 10):

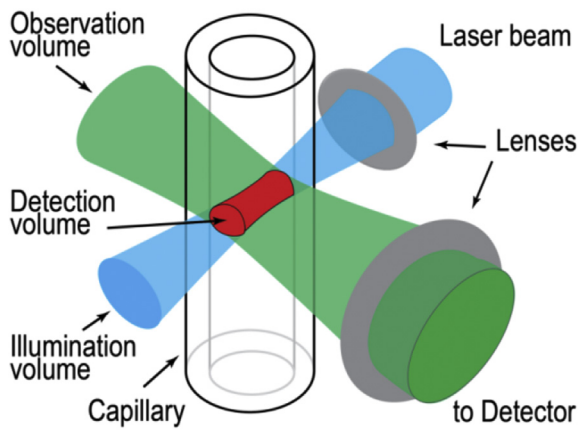

Fig. 9. Spatial filtration by intersection of observation and illumination volumes. Detection volume is defined as illuminated volume in the field of view of detection system.

$$d = \frac{K\lambda}{NA}, \tag{13}$$

where d is a diameter of the Airy disk (central bright disk of circular diffraction image [79]) in case of uniform lens illumination or a diameter measured at the $1/e^2$ intensity level in case of the Gaussian laser beam; λ is the wavelength of light; K is a constant equals to 1.22 for the uniform illumination, 0.82 for the Gaussian beam, or 0.915 for the Gaussian beam truncated by lens aperture D at the $1/e^2$ intensity level [80]; and NA is the numerical aperture.

NA is an objective lens characteristic that describes the cone in which the lens can accept or emit light:

$$NA \equiv n \sin\psi = n \sin\left(\arctan\frac{D}{2F}\right) \approx n\frac{D}{2F} \text{ (for small } \psi), \tag{14}$$

where n is medium refractive index; ψ is the half-angle of the light cone (see Fig. 10a); D is diameter of the light beam (aperture stop of lens); F is focal length of the lens.

Let us consider a typical convex lens with a diameter of 2.5 cm and a focal length of 5 cm. According to Eq. (14), maximum NA of this lens is 0.25. In a detection channel, the lens collects light in a solid angle of 0.2 steradian and it can take only 1.5% of the light emitted by a point source that is located in the focus (see Collection efficiency at Fig. 11). As a result, a standard optical lens doesn't provide efficient light collection, and in sensitive CE-LIF, the use of high-NA objective lenses is preferable. If we place such a lens in the excitation channel, then according to Eq. (13)–(14) and Fig. 10b, a blue laser beam with a typical diameter of 0.7 mm [39,81] will have a waist of about 57 μm at the lens focus, which is comparable with the ID of typical capillaries, and this ordinary lens may be useful for excitation. Note, the waist size may be adjusted both by expanding the laser beam diameter and by changing the focal length of the lens (see Waist diameter at Fig. 11).

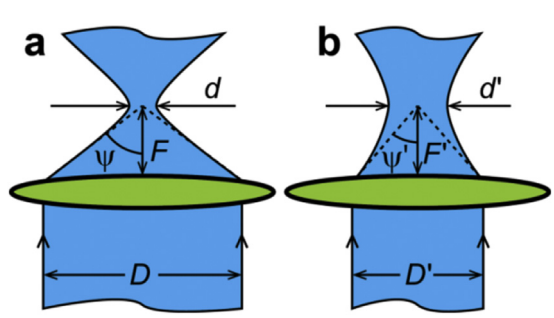

Fig. 10. Light focusing by objective lens. (a) Minimal beam waist d at the focal plane is limited by light diffraction and given by Eq. (13). (b) Lens with partly illuminated back aperture has smaller actual NA and a larger beam waist.

5.1.2. Right angle configuration

There are different mutual arrangements of an excitation source, a capillary, and detectors with the main goal to efficiently excite sample and collect luminescent light while avoiding scattering and other contributors to background [82,83]. Fig. 9 shows a simple optical scheme where one objective lens is used to deliver excitation light onto a capillary and another objective lens collects fluorescent light conventionally at a right angle to the excitation direction. This scheme is very popular in CE-LIF because it is simple and realizes spatial confinement by the orthogonal intersection of the excitation beam and the field of view of the fluorescence-collection optics.

Microscopy objective lenses with high-numerical aperture have to be utilized for precise focusing of the laser beam onto the capillary core and for efficient collection of fluorescence (Fig. 11). Such objectives usually have short working distances with large outer dimensions, for example Olympus LUCPLFLN (60×, $NA = 0.7$) has working distances ~2 mm with the body diameter of 26 mm. For the configuration with two lenses, shown in Fig. 9, there is a lack of space for both of them in close proximity to the capillary. Moreover, the maximal numerical aperture (NA ~ 1.3–1.4) is exclusively available for lenses with immersion liquid, and these lenses could not be used in the described scheme, as they have even smaller working distances of a few hundred microns. As a result, the main drawback of the right-angle configuration is the requirement that only "dry" objectives be used limits light-collection efficiency, which makes its application in highly-sensitive CE-LIF devices less attractive.

5.1.3. Epi-illumination configuration

Epi-illumination configuration, where a single lens is used to focus an excitation laser beam and to collect fluorescence emission,

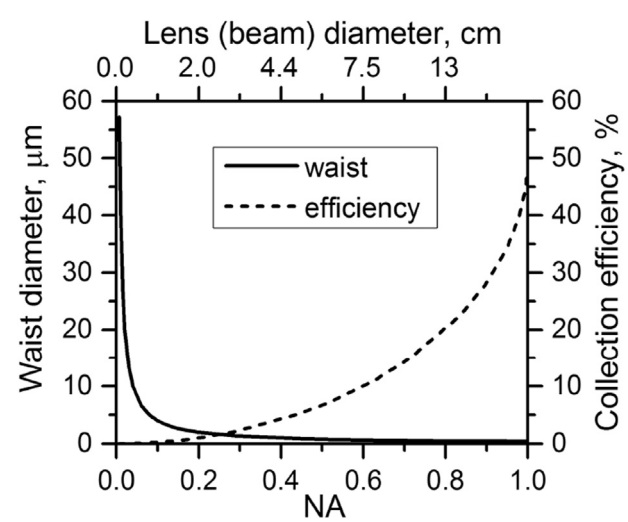

Fig. 11. Fluorescence collection efficiency of a "dry" lens as a function of numerical aperture (dotted line). Waist size of light beam focussed by the lens with a focal length of 5 cm as a function of the beam diameter (solid line). Waist was calculated with Eqs. (13) and (14) where NA was determined by using either a lens diameter (for uniform illumination) or a laser beam diameter (in case of partly illuminated lens (see Fig. 10b)).

allows placement of the high-NA objective lens in close proximity to the capillary in a CE-LIF setup (Fig. 12a) [84]. Immersion objective lenses significantly improve light-detection efficiency. A typical oil-immersion objective lens with $NA = 1.4$ corresponding to a half-angle ψ of ~67° gathers up to 30% of light emitted by a fluorescent sample.

In epi-illumination configuration, the spatial filtration is employed by inserting a pinhole (field aperture) at the intermediate focus in the detection channel (Fig. 12a). This confocal pinhole, confines the detection volume decreasing both field of view (in transverse direction) and depth of focus (in axial direction) (Fig. 12b), and helps to collect signal from only the hollow part of the capillary. Dimensions of the detection volume depend on the pinhole size and reach a minimum when the pinhole size is equal to or smaller than the diameter of the Airy-disk image at the pinhole plane. In such a case, the optical resolution (lateral and axial) defines dimensions of the minimal detection volume.

Lateral resolution (or the diameter of Airy disk) for the confocal system, in which foci of illumination and observation objectives coincide, can be described by Eq. (13) with $K = 0.88$ for the uniform lens illumination [85]. Moreover, in the confocal diffraction pattern, the light energy is almost entirely contained in the central Airy disk without subsidiary rings, which significantly improves contrast and further facilitates the lateral confinement of the detection volume.

The depth of focus (sometimes called axial resolution) can be measured by moving a sample through the focal point and plotting the signal as a function of the axial position. As result we get a bell-like signal curve, and the full width at half maximum intensity ($FWHM_{\text{axial}}$) is usually used as a figure of merit of the depth of focus. In the case of (i) confocal pinhole with Airy-disk limited size, (ii) uniform lens illumination, and (iii) equality of excitation and fluorescence wavelengths, the axial resolution of flat fluorescent sample is determined by Eq. (15) [86]:

$$FWHM_{\text{axial}} = \frac{0.67\lambda}{n(1-\cos\psi)} \approx \frac{1.34n\lambda}{NA^2} \text{ (for small } \psi), \tag{15}$$

Under the assumption of aberration-free optics, with green laser excitation, and using Eqs. (13) and (15), we may represent the minimal detection volume as an ellipsoid of 300 nm in diameter and 400–500 nm in length. Note, that Eq. (13) defines a transverse size of point spread function at zero intensity level while Eq. (15) gives an axial length at the level of 50%. The minimal detection volume in reality is greater than the calculated one, but it is still too small to be suitable for CE-LIF applications, which typically utilize capillary with ID substantially larger than 2 μm as we have already discussed in Chapter 1. To enlarge the dimension of the detection volume up to capillary ID and consequently to observe all migrating molecules through the capillary, it is necessary to increase the diameter of the pinhole in the detection channel. Also, the waist of the illumination beam should be tuned to match the increased observation volume.

When the pinhole size is much larger than the value used for getting the diffraction limited resolution, geometric optics rules can be applied for calculation of diameter of detection volume, which is connected with pinhole size through the magnification M of the optical system. Note, that in this case, lateral resolution, which defines the sharpness of detection-zone boundaries in the focal plane, should not deteriorate because this resolution is defined only by the wavelength and NA of the lens. The depth of focus increases with growth of the pinhole diameter and may be estimated through the axial range resolution d_z, which, in case of laser excitation, is calculated using optical magnification M and pinhole diameter Ph [86]:

$$d_z = \frac{n\,Ph}{\sqrt{2}\,M\,NA}, \tag{16}$$

It should be noted that increasing the pinhole size in the detection channel enlarges only the volume observed by the detector, while the volume excited by the laser remains unchanged. To increase the illuminated volume it is necessary to expand a waist d' of the focused excitation beam by reducing the diameter of the laser beam D' (Fig. 10b) or by defocusing laser beam inside the capillary.

The above described estimations of detection-volume size are valid only in the absence of aberrations in the optical system. Otherwise, the detection volume cannot be easily estimated (see Fig. 8 and Section 4.3). High-NA objectives (both dry and immersion) are designed for use with a coverslip. So, to minimize optical aberrations, a coverslip should be present and its thickness (usually 0.17 mm, No 1.5) must be controlled [79].

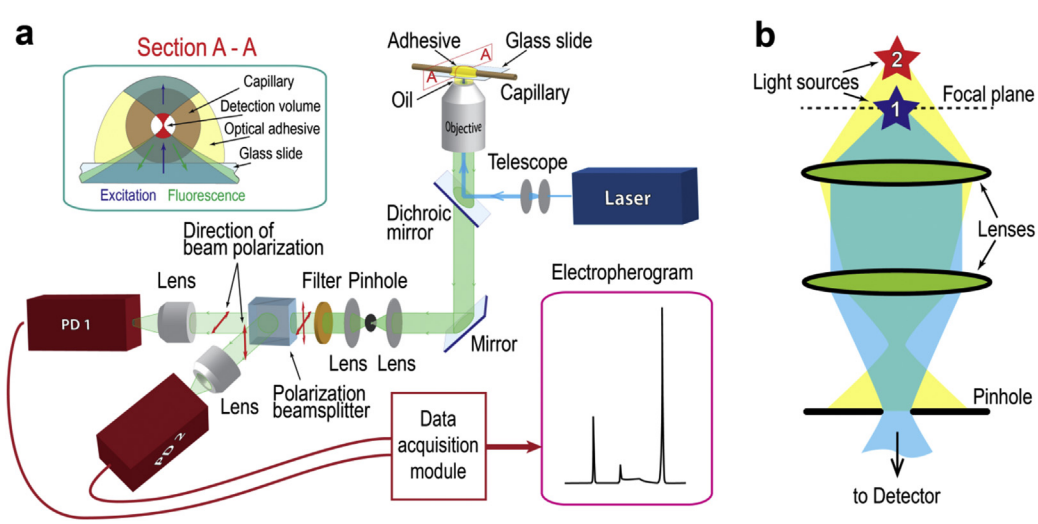

Fig. 12. (a) Schematic of epi-illumination confocal configuration in a CE-LIF setup (adaptation from Refs. [59,64]). "Epi" means that illumination and detection is done from one side of the sample. The inset shows a detailed cross-section of the capillary, which is glued to a glass slide with an optical adhesive. Such approach is used for easy and precise positioning the capillary in the focus of high-numerical-aperture objective and for decreasing beam distortion by use of a properly selected refractive index of the adhesive. (b) Function of confocal pinhole. Only light from source 1 can fully pass to the detector. Light from source 2, which is positioned out of the focal plane, is filtered by the pinhole.

A large detection volume matching the capillary ID is required to observe all analyte molecules passing through the capillary cross-section. On the other hand, the large-volume detection suffers from the increased optical background, whereas a peak resolution of the CE method deteriorates. To overcome this contradiction a detection volume of a disc shape should be utilized. In this case, we can significantly reduce the detection volume in the direction along the capillary axis while maintaining observation of all fluorophore molecules in a stream. An optimized configuration was realized using cylindrical optics in the excitation channel and confocal slit in the detection channel [21]. Rectangular illumination area of 2×0.5 μm, which is diffraction-limited in one direction, was created to match a microchannel width of 2 μm. Overall detection efficiency of 94% was achieved for single Alexa Fluor® 488 dye molecules [21].

5.2. Spectral filtering

An excitation source should provide a light beam of narrow spectral band. However, laser emission may contain the light of laser-medium pumping, residual radiation of additional harmonics (solid-state lasers), luminescence of laser materials (compact solid-state and diode lasers), and plasma lines (gas lasers). Currently, in the excitation channel of a CE-LIF setup, laser light may be readily refined due to the high quality and available variety of modern bandpass filters [37]. Note that glass substrates of bandpass filter can luminesce under intense laser irradiation. In such a case, a series of dielectric mirrors selectively reflected only laser line might be needed to clear the excitation spectrum.

The real challenge of spectral filtration is to separate useful fluorescence signal from the total light generated inside the capillary. As it has been noted in Chapter 1, the main source of optical background in CE-LIF is elastic Rayleigh scattering of laser light and inelastic Raman scattering mainly from water molecules. Usually the experimenter chooses a fluorescent dye with a large Stokes shift, *i.e.* fluorescence spectrum is sufficiently far from excitation wavelength. In this case, bandpass optical filters may successfully block Rayleigh and major part of Raman scattered light. Advanced emission bandpass and cut-off filters eliminate necessity of additional expensive notch filters for laser line suppression [37]. Moreover, in the epi-illumination configuration, a beam-splitter facilitates separation of laser light and dye luminescence. One simple trick helping to remove Rayleigh's scattered light is a slight disalignment in the optical scheme, when the capillary is slightly shifted (on the order of several microns) out of the laser trajectory, causing the scattered light to be successfully rejected by the pinhole [87]. This disalignment reduced fluorescence intensity by 25.7% but resulted in an overall SNR improvement of 8.3 times compared with that for unshifted capillary.

Although light scattered by water molecules and auto-fluorescence of BGE are the main sources of background signal in CE-LIF, it is necessary to take into account the optical signals generated by other media, which fall within the detection volume, *e.g.* capillary glass, immersion liquid of the objective lens, or coverslip glass. Contribution of these additional background signals depends on how well the detection volume fits the capillary core. Optical grade glass and fused silica are transparent in the visible region to the naked eye. Nevertheless, when applying highly-sensitive detection technique, there is a high probability to observe weak emission from some apparently-transparent optical elements, which still absorb light slightly in the UV–vis region and fluoresce in the detection window under blue laser excitation. For example, capillary walls made of fused silica may both scatter excitation light and cause background luminescence similarly to a solvent in BGE (see Chapter 7). Fig. 13 demonstrates the main features of scattered light by fused silica as well as by water. We plotted nonpolarized Raman spectra taken from Refs. [88–91] to indicate position and relative intensities of scattered light. For possible polarization issues (excitation, detection, and geometry) see the following review [92] and use polarized Raman spectra [93,94].

Raman scattering due to water environment should be considered more carefully, because this phenomenon greatly limits SNR for fluorescence studies of intact biomolecules. For the conditions described in Chapter 4, the ratio of the number of useful photons to scattered ones is only about 3–4 times when a single molecule is placed in the considered excitation volume (Section S1 in Supplementary Material). If we assume ideal light collection, Poisson statistics for scattered background light, and the absence of other background sources; then one detected molecule provides *SNR* of about 121 (Section S1 in Supplementary Material). A real SNR value will be lower because of the impact of both silica Raman lines (Fig. 13) and impurities' luminescence (see Ref. [95] as an example).

Spectral filtration allows us to collect fluorescence of different fluorophores into separated detection channels. Lasers with different emission wavelengths may be required for the simultaneous excitation and analysis of multiple analyte components in a CE-LIF setup [96,97].

Spectral filtering is the most obvious method to reduce the optical background. It is used in every CE-LIF setup, and in many cases, spectral filtering is sufficient to obtain acceptable SNR value.

5.3. Lifetime filtering

Time-resolved detection measures the intensity of optical signal as a function of time following a short excitation pulse [98], and it may be implemented in CE-LIF analysis. In this method, a pulse laser creates a train of pulses at a high repetition rate (usually of tens of MHz). In the fast time scale (at times shorter than pulse period), the signal represents a curve having a fast rise during the excitation pulse and a slow decay with the relaxation time being equal to the fluorescence lifetime, typically in the nanosecond time range. In the long time scale (seconds and minutes) associated with the CE measurement, the detector observes a chain of short optical signals. These individual kinetic signals have to be averaged and/or integrated over specified time intervals for the subsequent data treatment. The choice of time intervals for averaging/integrating depends on the injected plug shape and length, for example, integration (binning) time was equal to hundreds of milliseconds to gain an optimal SNR value in Ref. [64]. There are two implementations of the lifetime-filtering technology: *time-gating* and *lifetime-determination methods*.

In the *time-gating method*, signal is acquired (or rejected) only within a predefined time window. In this way, the SNR value can be improved for the electrophoretic signal, even when the spectral filtering fails, *e.g.* in presence of intensive Raman scattering at the wavelength of fluorescence [44]. Analyte fluorescence is separated from scattered light because these signals occur in different time-scales: time-dependence of both Rayleigh and Raman scattered light coincides with the duration of excitation pulse, whereas fluorescence of commonly used organic dyes decays in a few nanoseconds after the end of the excitation pulse. At the current stage of technology development, lasers may generate short sub-nanoseconds pulses practically at any wavelength exploited in CE-LIF [39]; fast (picosecond) and sensitive photodetectors have also been developed [99–101]; and time-correlated single-photon counting electronics is available in compact modules and boards [81]. Therefore, it is no longer difficult (but still expensive) to separate useful fluorescence from scattered light using time-

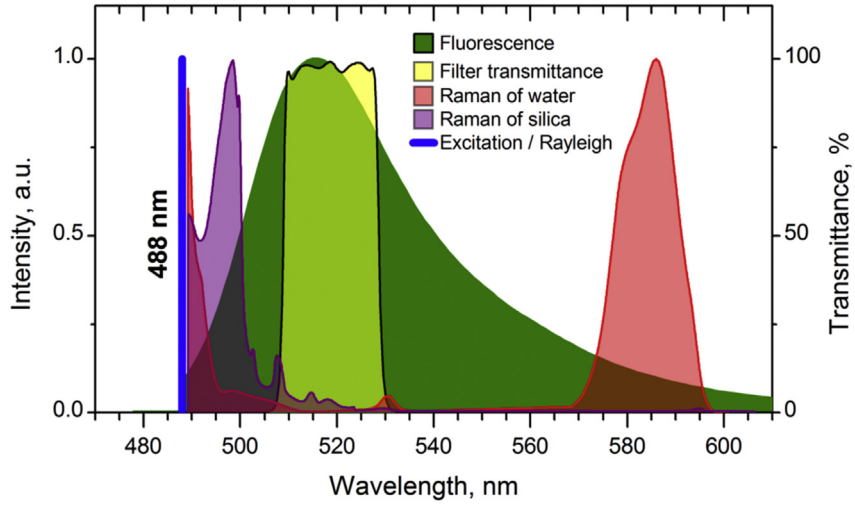

Fig. 13. Normalized emission spectrum of fluorescein in water (green). Simplified plot of arbitrary Raman intensities *vs* wavelengths for a 488-nm excitation line for water (pink) and silica (purple). Transmittance of Semrock FF01-520/15 bandpass filter (yellow). Raman spectra are based on data from Refs. [88–91]. (For interpretation of the references to color in this figure legend, the reader is referred to the web version of this article.)

resolved detection. Fig. 14 shows signal-rejecting window applied to the fluorescein signal. The initial part of time-resolved signal within 0.4 ns was removed, which promoted a SNR improvement of 30% [59,64].

High-quality bandpass filters with sharp transmittance spectra allow selecting an optimal wavelength range for fluorescence detection and good suppression of scattered light. Consequently, for modern sensitive CE-LIF detection, the role of other sources of optical backgrounds (*i.e.* autofluorescence of BGE, capillary and coverslip materials, and immersion oil) are becoming more relevant. As can be seen in Fig. 14, the autofluorescence decay curve of the buffer is non-exponential with an average time constant of about the same order of magnitude as the lifetime of fluorescein. In this case the *time-gating method* can only remove the scattering portion of the optical background but not the autofluorescence. The situation can be improved by using a fluorescent probe with a long

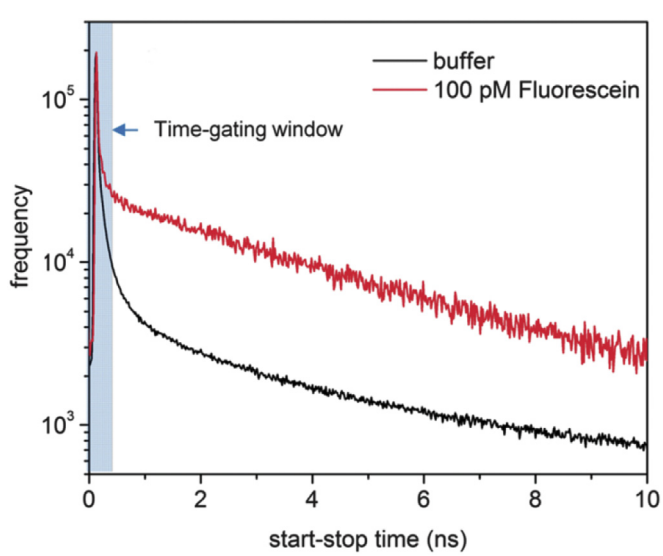

Fig. 14. Lifetime filtering in CE-LIF. Time-gating window of 0.4 ns is applied to fluorescence decay curve of fluorescein with a lifetime of 4 ns to reject light scattering signal. SNR improvement is approximately 30%. Reproduced from Ref. [64] with permission from The Royal Society of Chemistry.

lifetime of tens of nanoseconds, but currently there is a lack of organic dyes with both long lifetimes and high fluorescence quantum yields. Millisecond-long luminescence of lanthanide chelates [102] and phosphorescence of the enantiomers of chiral compounds [103,104] were proposed for time-gated setups; however, insufficient quantum yield of these probes does not allow one to improve LOD.

In the *lifetime-determination method*, fluorescence decay curves, which are measured for individual CE peaks, may be readily fitted by a model function to determine lifetimes of fluorescing species in the plug [105]. Fluorescence lifetimes help to identify multiple analytes in CE-LIF facilitating dye multiplexing [106–108]. Potentially, the *lifetime-determination method* can be applied for SNR improvement by extraction the useful signal with a known fluorescence lifetime from the background signal with non-exponential decay. To successfully exploit the *lifetime-determination method* the acquired kinetic signals should have low noise and fluorescing species should be characterized by significantly different lifetimes.

Pulse lasers working at high repetition rate are the main excitation sources for the lifetime-filtering technique. Caution should be taken while working with the pulse excitation, since the optimum excitation level might be different for pulse and continuous wave (CW) modes. For the same two-level system as in the 1st part of Section 4.2, a temporal expression for the ratio between the number of molecules in the excited state to the total number of molecules in the excited volume follows (Eq. (S19) Supplementary Material):

$$r = \frac{\theta I_0 \phi_f}{k_f + \theta I_0 \phi_f}\left(1 - \exp\left\{-t\left(k_f \big/ \phi_f + \theta I_0\right)\right\}\right), \tag{17}$$

which is similar to Eq. (11) except for an additional temporal multiplier, and I_0 being the power density during the pulse duration. Let's consider a pulse laser with a 1 mW average power. The pulse power will be 1 W for 100 ps pulses emitted at a 10 MHz rate, which, according to Eq. (17), results in ~9% of all fluorescein-like molecules being in the 1st excited singlet state. For such molecules and with negligible triplet state formation, 1 mW CW-mode laser results in 0.4% population of the excited state based on Eq. (11). The difference in levels of excitation between the pulse and CW-modes is more than an order of magnitude and may lead to a

higher rate of analyte photodamage in the pulsed experiments. In case of 10 μm capillary and 1 mW power, an average power density is about 1 kW cm^{-2}, and such excitation conditions did not lead to difference in Rhodamine 6G photobleaching between CW and picosecond-pulse excitation [109]. But in general, interaction of fluorophore molecules with the very powerful femto-, pico-, or nanosecond light pulses is quite complex and often results in increased probability of photobleaching [110–112], which may lead to decreased SNR in CE-LIF.

Spectral filtering successfully suppresses both Rayleigh and Raman scattering but it is usually accompanied by significant narrowing of detected fluorescence spectrum. Lifetime filtering may be used together with only Rayleigh-scatter attenuator (laser-line notch filter) that allows detection of the whole fluorescence spectrum of the fluorophore. Signal induced by the transmitted Raman light can be easily removed by time-gating method. This approach is useful for highly-sensitive measurements where all fluorescence photons should be collected.

5.4. Use of polarization

Polarization anisotropy carries information about the fluorophore properties such as molecular orientation, aggregation, rotational diffusion *etc.* [105,113]. Under illumination by linearly polarized light, the fluorophores are preferentially excited, when they have absorption transition dipole moments parallel to the electric field vector of light. Rotational diffusion changes the orientation of molecules in space. If the rotational relaxation time is shorter than fluorescence lifetime then the direction of polarization of the emitted photon will be different from that of the absorbed photon. Anisotropy $\bar{r}$ reveals the angular displacement of the fluorescent molecules, which occurs during the lifetime of the excited state:

$$\bar{r} = \frac{I_{\parallel} - \overline{G} I_{\perp}}{I_{\parallel} + 2\overline{G} I_{\perp}}, \tag{18}$$

where $I_{\parallel}$ and $I_{\perp}$ are parallel and orthogonal components of the fluorescence intensity, respectively, which are measured by separate photodetectors (see Fig. 12a); $\overline{G}$ is a correction factor of sensitivity differences of the photodetectors [105]. Eq. (18) is usually applied for typical CE-LIF instruments, while for confocal scheme with high-NA microscope lens an additional correction for lens depolarization may be required [114].

The anisotropy associated with rotational diffusion of molecules allows us to distinguish analyte molecules moving freely in the flow both from the analyte molecules adsorbed on surface of the capillary walls and from other emitting point sources inside the wall glass. Thus, the measurements of fluorescence anisotropy $\bar{r}$ may theoretically serve as an additional analysing tool for discriminating analytical signal and, thus, improving SNR. However, we are not aware of any documented works which used fluorescence anisotropy for optical filtering in CE-LIF detection.

Selection of the optimal polarization mode for excitation light may help to supress light scattering by capillary in CE-LIF measurement. Polarized light is known to have different efficiency of reflection from dielectric media depending on the orientation of polarization vector towards the incidence plane. If a linear polarization of excitation light is used and the capillary is perpendicular to the optical axis of the objective lens, as in the confocal CE-LIF configuration, an excess in backward reflection from capillary walls may be observed for certain directions of the polarization vector. To reduce this reflection the common rule is to align polarization vector of excitation light and capillary cross-section plane, which arises as an intuitive consequence of Fresnel equations and is proved by numerical calculations for a round capillary [115]. If the setup configuration is distinct from the above-mentioned, then an experimental test may help to find an appropriate angle between the polarization vector and the capillary axis.

5.5. Additional filtering techniques

Some approaches based on signal coding and advanced data treatment may be adopted in CE-LIF from electrophoretic techniques performed on microchips. For example, the cross-correlation injection-detection technique uses multiple injections which are performed in a continuous but random sequence. Subsequent mathematical treatment allows us to quantify analytes from ultradilute solutions with picomolar LODs [116]. An approach which takes advantage of multiple-point detection and subsequent Fourier transform was implemented to convert time-domain electropherograms into frequency-domain plots [117]; though, this approach could reliably detect analyte solutions of only micromolar concentrations.

Along with optical filtering that minimized background luminescence, additional filtering of the electrical signal is used for reduction of high-frequency noise and long-term baseline drift. For the analog detection mode electronic low-pass filters readily rejects a big portion of the thermal noise by adjusting filter's cut-off frequency with the minimal sampling rate [118]. In practice, the actual sampling rate is at least twice higher than the adjusted cut-off frequency to facilitate further digital filtering [119,120]. With the advent of computers, digital filtering has been replacing electronic filters, helping to reject baseline noise as well as peak finding and quantification [46]. Useful digital techniques for noise removal include convolution filtering (Savitzky–Golay and moving average filters), median filtering, and Gaussian smoothing, Fourier and wavelet transforms [121–125]. Digital filtering of acquired electrophoretic signal is rather simple and widely-used method to improve SNR.

6. Detection

A detection system of a typical CE-LIF instrument consists of both optical and electronic parts. In the optical part, analyte fluorescence is collected and transmitted to an optoelectronic transducer where light is converted into electrical current. The electrical current is then transformed into “intensity *vs.* time” dependence by signal processing electronics and a readout system to produce an electropherogram. In CE-LIF, two major categories of transducers are used: i) photomultiplier tubes (PMT), and ii) semiconductor detectors, such as avalanche photodiodes and multichannel arrays. Note that all of these photodetectors measure incident photon rate rather than photon energies.

6.1. Collection optics

To get the best detectability, LIF-detection optics should collect maximum of light, which is isotropically emitted by fluorophore molecules. There are numerous practical solutions of this complicated technical task, for example, the system with two microscopy objectives collecting light from two sides of the detection volume [27], silver mirror coating of one capillary side to reflect fluorescence into a single objective lens (Fig. 15) [126], optical fiber bundle with input ends radially distributed around the capillary [127], and spherical mirror as high-numerical-aperture objective [128].

Ball lenses demonstrate a high NA value up-to 0.8. Several authors reported the ability of a ball lens to successfully substitute objective lenses with high NA for focusing excitation as well as

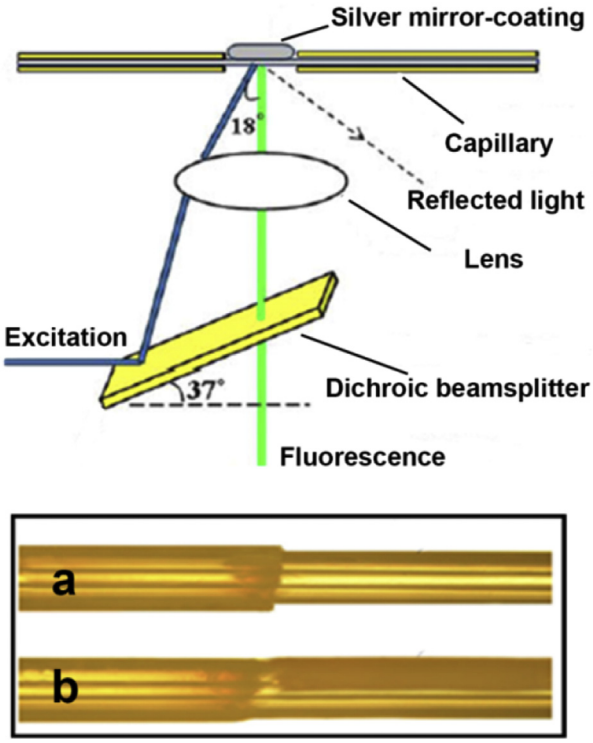

Fig. 15. Schematic of CE-LIF detection with silver-coated capillary to increase fluorescence collection efficiency. The inset shows pictures of the detection zone of an (a) ordinary capillary, and (b) capillary having the silver mirror coating. Adapted from Ref. [126]. Copyright© 2013 by John Wiley Sons, Inc. Reprinted by permission of John Wiley & Sons, Inc.

collecting fluorescence light, and impressive picomolar LOD values were obtained [129,130]. A sapphire ball lens touching the capillary combined with a concave reflector positioned at the opposite side may give a total light-collection efficiency of up to 40% [131]. A similar to that optical schematic is employed in an LIF detection of a P/ACE™ MDQ Plus Capillary Electrophoresis System manufactured by SCIEX.

6.2. Photomultiplier tubes

A photomultiplier tube is a vacuum device incorporating a photocathode, an anode, and a number of multiplication electrodes, called dynodes. PMT's photocathodes may generate a photoelectron in a response to a single photon, and dynodes multiply this photoelectron 10^5–10^8 times (value of gain, *g*) resulting in a detectable charge packet. A PMT can operate in both analog and photon-counting modes. In the analog mode, an illuminated PMT outputs a current signal resulting from the continuous arrival of many anodic pulses. An electronic integrator with a time constant larger than the pulse duration is used to get the continuous anodic current. In the photon-counting mode we may literally count every separate photon striking the photocathode through counting charge packets containing *g* electrons. In this mode, the intensity of light hitting the detector is transformed directly into an electric pulse count-rate.

The high gain of PMTs makes this type of photodetectors very popular for low-light-level detection. The gain could be changed by adjusting voltage, thus PMT must be utilized with very stable power supplies to provide reliable signal output. Careful control over the light level and PMT gain is required to keep the anode current in the linear range. Modern power supplies and voltage dividers prevent bias of dynode potentials and nonlinearity caused by space-charge effects in the last dynodes; therefore, PMT can be utilized as long as the anode current does not exceed a maximum value (*e.g.* 0.1 mA for Hamamatsu R928) [132].

Dark current in PMTs primarily arises from the thermal emission of the photocathode (or early dynodes). For extremely low light levels, noise of the dark current (mainly shot noise) can limit the LOD. In such a case, cooling the PMT down to −30 °C and even below helps to decrease the dark current considerably [132]. For on-capillary detection the photocurrent induced by the optical background is usually much larger than the dark current of PMTs. So, the PMT-based noises are usually minor components of the total noise in CE-LIF measurements.

PMT designs which rely on the emission of photoelectrons from a photocathode, *i.e.* on the "external photo effect", have an intrinsic limitation: quantum efficiency, *i.e.* the probability that a photon gives rise to a photoelectron, is always smaller than 50%. This is due to the fact that the photoelectrons are emitted from the photocathode surface in all directions and half of them are lost on the cathode. This drawback is almost eliminated in semiconductor photodetectors relying on the "internal photo effect" with a theoretical quantum efficiency of 100%. And such a high quantum efficiency of a detector along with high-performance light collection is necessary to achieve the highest sensitivity of CE-LIF detection.

PMTs usually have large photocathode areas (*e.g.* 8 × 24 mm for Hamamatsu R928), and it is very convenient for light collection and considerably simplifies the detection scheme. A very high amplification, a low dark noise and a reasonable sensitivity make PMT a detector of choice for most common fluorescence applications in UV–vis. PMTs may be also applied in the red and near-infrared spectral region, but their low quantum efficiency in this range needs to be taken into account. Detectors with the maximum possible quantum efficiency, *e.g.* avalanche diodes, may be required for measurements in which every emitted photon has to be counted.

6.3. Avalanche photodiodes

Specially designed semiconductor photodetectors can detect single photons, as a result of the efficient generation of a photoelectron and internal electron multiplication. A suitable multiplication of charge carriers is achieved by the "avalanche effect" [38], so a photodetector which operates in such a gain mode is called an avalanche photodiode (APD). APDs designed specifically for single-photon detection should have extremely large gain, and, thus, must utilize photon-induced avalanche breakdown with an active or passive quenching circuit for avalanche control [99–101]. This operation mode is often termed 'Geiger mode", and APD, working in Geiger mode, is named single-photon avalanche photodiode (SPAPD or SPAD). SPAD provides suitable multiplication of the 1st photoelectron to generate a trigger signal and, thus, to operate in the counting detection mode. SPAD, however, fails in analog mode of operation as every photon generates an avalanche of a random amplitude, and the integrated (analog) output signal responds nonlinearly to the number of incident photons [38].

The rate of thermally generated carriers in SPAD is very high; therefore, this type of detectors must be cooled. Even for cooled SPAD the dark-count rate is much larger than for a PMT with a similar photosensitive area. To minimize the dark-count rate SPADs are produced with very small photoactive zones of 10–200 μm in diameter. Small size of the photosensitive area is the main drawback of SPAD use in a typical fluorescence application, but it is not a significant problem for CE-LIF as the emitting volume inside the capillary is very small and comparable in size with the SPAD photoactive area [28,133]. Moreover, the confocal detection in this

regard has a very strong advantage because it utilizes focusing of fluorescence beam into a small aperture and can be easily coupled with SPAD [59,64].

6.4. Multichannel arrays

Semiconductor photosensitive arrays, such as charge-coupled devices (CCDs) and active-pixel sensors (*e.g.* CMOS sensor), can provide simultaneous multichannel detection of spatially distributed light beam. In scientific applications, CCD-based instruments are the most widely used for low-light-level detection. Improvements in electron-multiplying CCD (EMCCD) technology allow getting the electron gain up to levels comparable with commercial SPADs [134]. On the other hand, single-photon imaging detectors have been recently developed utilizing monolithic arrays of 1024 and 2048 SPADs [99].

Multichannel arrays are usually exploited in combination with spectrographs in order to observe fluorescence spectra. In spectral detection mode, light irradiation is dispersed over an array of pixels according to photon wavelength. A single pixel sensor is characterized by a poor SNR, but the whole-device SNR is significantly improved by signal integration from a large number of pixels. In the vertical pixel binning mode, there is an integration of signals from one column of pixels. This procedure can be applied because every vertical column of an array in the spectrograph focal plane is illuminated by photons of the same wavelength. If the spectral resolution is not necessary, horizontal column binning over a wide wavelength region is realized. The optimum wavelength interval for data acquisition has to include the fluorescence spectral band and omit the profiles of Rayleigh and Raman scattering, and such approach was successfully realized in wavelength-resolved CE-LIF detection [32,135]. In addition CCD-based CE-LIF setups can be advantageous in discriminating between individual analytes by measuring time-dependent wavelength profiles during electrophoretic separation [32,83]. This feature is particularly useful for improving the electrophoretic resolution of analytes in long injected plugs.

6.5. Modes of detection

Analog and photon-counting modes are two main types of signal detection in fluorescence measurements. In the analog mode, light constantly irradiates detector causing continuous current signal, which then should be processed (*e.g.* amplified, filtered) to make it suitable for digitizing by analog-to-digital converter (ADC). Modulation of the *dc*-signal and advanced processing of the *ac*-signal are desirable before the digitizing step for noise reduction [118]. Continuous electrical signal in the analog detection mode is transferred to the digital form by ADC with a certain sampling rate. From a physics point of view there is a minimal sampling rate which is two times faster than the highest frequency of the signal, and this rate ensures that the obtained set of digits is sufficient to reconstruct the initial analog signal [119,120]. In Chapter 4, we showed that typical time for a single molecule to pass a small excitation volume is about 10 ms, which means that the highest possible frequency of any detected processes under such separation is about 100 Hz. Therefore, in our case, single-molecule events should be acquired with a frequency of 200 Hz. On the other hand, if the width of detected CE-spikes is about 1 s then 2 Hz sampling should be sufficient.

CCD and CMOS sensors work only in analog detection mode, PMTs and EMCCDs may work in both analog and photon-counting modes, whereas commercial SPADs are utilized only for photon counting. In the photon-counting mode we may detect and count every individual photon striking the photodetector, moreover, the detector output is digital in the first place, eliminating the need for ADC. Signal processing consists of pulse-height discrimination and counting, resulting in a definite number of pulses (photons) during a preselected time interval. A discriminator passes only pulses, which are above a threshold level, which allows rejecting the electronic readout noise and some dark current pulses. It may seem that the use of pulse-height discrimination would always provide better SNR in the photon-counting mode than in the analog mode, but such SNR advantage is only significant under certain conditions. To estimate these conditions we consider SNR expressions for photon-counting and analog signal processing in PMT-based luminescence measurements. SNR for a photon counting detector is given by Eq. (19) [136]:

$$SNR_{\mathrm{pc}} = \frac{n_{\mathrm{S}}}{\sqrt{n_{\mathrm{S}} + n_{\mathrm{B}} + n_{\mathrm{d}} + (\xi n_{\mathrm{S}})^2 + (\chi n_{\mathrm{B}})^2}}, \tag{19}$$

where n_{S}, n_{B}, and n_{d} are numbers of analytical, background, and dark signal counts, respectively; ξ and χ are signal and background flicker factor (relative SD of fluctuations in photon flux due to flicker noise), respectively. SNR for an analog detector is given by Eq. (20) [136]:

$$SNR_{\mathrm{a}} = \frac{i_{\mathrm{S}}}{\sqrt{K(i_{\mathrm{S}} + i_{\mathrm{B}} + i_{\mathrm{d}}) + (\xi i_{\mathrm{S}})^2 + (\chi i_{\mathrm{B}})^2 + \left[\frac{(\sigma_{\mathrm{d}})_{\mathrm{ex}}}{gG}\right]^2 + \left[\frac{\sigma_{\mathrm{ar}}}{gG}\right]^2}}, \tag{20}$$

where i_{S}, i_{B}, and i_{d} are the current of analytical, background, and dark signal, respectively; K is a bandwidth constant equal to $2e\Delta f(1+\delta)$, e is electron charge, Δf is noise equivalent bandpass, δ is a fraction of the quantum noise in the anodic current (usually 0.1–0.5); $(\sigma_{\mathrm{d}})_{\mathrm{ex}}$ is SD of the dark current excess noise which arises from non-thermal sources, σ_{ar} is SD of the amplifier-readout noise; g is PMT gain; and G is gain of current-to-voltage converter.

Shot or quantum noise is a fundamental noise that arises from photon nature of light. According to the Poisson distribution the shot-noise SD equals the square root of the number of photons. Flicker noise is non-fundamental (excess) noise for which SD of noise is directly proportional to the magnitude of the signal. Flicker noise is caused by fluctuations in experimental variables (*e.g.* excitation photon flux or temperature) due to imperfect instrumentation. Table 2 explains the nature of the noise components that are used in Eqs. (19) and (20).

It is possible to compare SNR of photon-counting and analog signal processing for these experimental conditions using Eqs. (19) and (20), and relationship between the current i and the number of counts n [136]:

$$i = \frac{2e\Delta f}{f_{\mathrm{d}}} n, \tag{21}$$

where f_{d} is a fraction of pulses which passed through the discriminator.

Three different scenarios with corresponding SNR relations may be considered.

Scenario A is a case when measurements are *limited by flicker noise* (in analytical or background signal), and consequently $SNR_{\mathrm{pc}} = SNR_{\mathrm{a}}$. It means that the type of signal processing does not influence SNR when flicker noise dominates.

Scenario B describes measurements *limited by shot noise* (in analytical or background signal or because of photocathode-thermal-emission dark current). When any type of shot noise dominates, we get the following relation:

Table 2
Components of the detector noise depending on detection mode and signal type.

Detection mode	Analytical signal		Background signal		Dark signal		Noise of amplifier-readout system
	Shot noise	Flicker noise	Shot noise	Flicker noise	Shot noise	Excess noise	
Photon-counting	$n_S^{0.5}$	ξn_S	$n_B^{0.5}$	χn_B	$n_d^{0.5}$	–	–
Analog	$(Ki_S)^{0.5}$	ξi_S	$(Ki_B)^{0.5}$	χi_B	$(Ki_d)^{0.5}$	$(\sigma_d)_{ex}/(gG)$	$\sigma_{ar}/(gG)$

$$\frac{SNR_{pc}}{SNR_a} = \sqrt{f_d(1+\delta)} \tag{22}$$

SNR_{pc} is typically 5–25% larger than SNR_a, if the discriminator coefficient f_d equals 1. Note, that $SNR_{pc} < SNR_a$, if the discriminator level is set too high and a large fraction of genuine counts is filtered out ($f_d < 1$).

In *Scenario C,* analog-signal processing is *limited by amplifier-readout or excess dark current noise.* For this scenario $SNR_{pc} > SNR_a$. Photon-counting signal processing is very useful for low-light-level measurements where analog signal processing is limited by excess-dark-current noise, dynode-thermal-emission noise, or amplifier-readout noise. Photon-counting mode has an advantage for long integration times because of tolerance to slow drifts in dc-offset levels and amplifier gains.

The optical background is the main source of noise in analytical signal at low analyte concentrations for the on-capillary CE-LIF detection. If flicker noise is eliminated by careful instrument optimization, then *Scenario B* is established and the relation of SNRs is described by Eq. (22). It means that photon-counting signal processing has a slight advantage over analog signal processing in highly-sensitive on-capillary CE-LIF.

In the case of experimental conditions described in *Scenarios A* and *B* the variation of the gain factors g and G (*e.g.* by PMT high-voltage tuning) has an insignificant influence on SNR in the analog detection mode as resulting from Eq. (20). This important conclusion is useful for the practical implementation of PMT-based detection.

6.6. Dynamic range

Dynamic range is also an important parameter of any detection system. It is determined as a ratio between the maximal and the minimal detectable signals. A linear dynamic range of a conventional PMT in the analog signal processing is rather wide, more than 5 orders of magnitude (Fig. 16) [137], so the detection system is usually limited by the dynamic range of ADC. A typical 16-bit ADC has a dynamic range of 4.5 orders of magnitude if the noise signal is set equal to the least significant digit in the ADC. Note that signal integration and averaging can increase the ADC dynamic range.

The dynamic range in photon-counting mode is limited under the condition of high count rates by the dead time of the photodetectors. The detector does not respond to subsequent photons for a small, but finite, time interval after the detection of one photon. This dead time correlates with the anode pulse width in PMT or with the duration of the avalanche quenching in APD. Dead time is about 5 ns for conventional PMTs and 50 ns for commercial SPADs [69,132]. The linear dynamic range of a detection system in photon-counting mode can be as small as 3 orders of magnitude [137]. This drawback of photon-counting detection for steady-state fluorescence measurements has been successfully overcome by employing cascaded APD counters connected in series to generate signals of different degree of attenuation [28,133]. As a result, the dynamic range for CE-LIF was expanded up to 9 orders of magnitude.

To conclude, in CE-LIF, it is possible to work efficiently in both analog (with PMT) and counting (with PMT and SPAD) modes. The only absolute necessity for the photon-counting mode is in time-resolved measurements, because the majority of fluorescent labels have lifetimes (several nanoseconds) which are too short for reliable determination by analog apparatus.

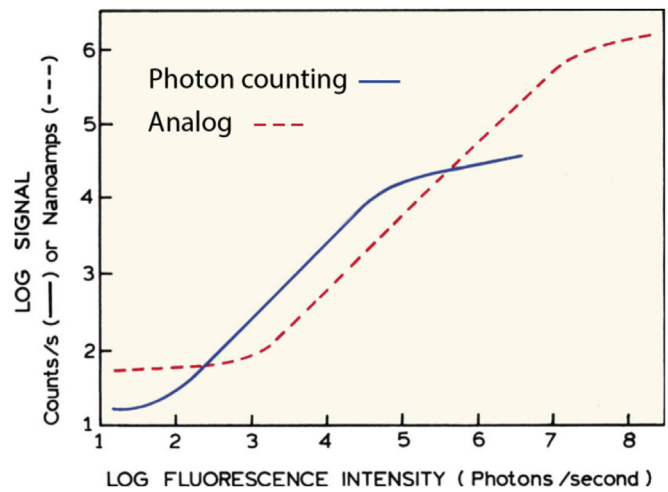

Fig. 16. Dynamic range of PMT in analog and photon-counting detection modes. Adapted from Ref. [137] with permission from Joseph R. Lakowicz.

7. Fluorescent labels and sample preparation

Derivatization is a common approach to modify analytes to give them more suitable analytical characteristics for both high-sensitivity and high-resolution in CE analysis [138–140]. For example, a generic nature of derivatization approach allowed creation and further development of a direct quantitative analysis of multiple miRNAs [14,58,141,142]. Fluorescent labeling is the major derivatization technique employed in CE-LIF. Organic dye molecules seem to be the best labels due to their properties: distinct fluorescence in the visible region, good photostability, small hydrodynamic radius in comparison with typical biomolecules to preserve electrophoretic mobility of analyte molecules after labeling [143].

Fluorescein derivatives are very popular dye-labels due to their high molar absorption coefficient ($\varepsilon \sim 8 \times 10^4$ M^{-1} cm^{-1} [57,62]), high fluorescence quantum yield ($\phi_f = 0.93$ [62]) and almost no shift of λ_{ex} and λ_{em} after reaction with different analytes, though, their fluorescence is sensitive to pH. Fluorescein has poor photostability, as a result, chemists continue to develop new fluorescent dyes to establish the next generation of improved organic fluorescent labels. Alexa Fluor® is a series of modern dyes with optimized properties, whose absorption and emission spectra cover the entire UV–vis range and resemble fluorescence characteristics of many common dyes [144]. Good photostability and insensitivity to a broad range of pH conditions are the main advantages of Alexa-dyes, especially over fluorescein derivatives. ATTO is another novel series of dyes with favorable properties for fluorescent labeling [145]. A successful attempt has been made by the Wolfbeis

group in the field of protein label development [146]: a new family of Chromeo™ dyes was created, which undergo a significant color change after covalent binding to proteins. Moreover, Chromeo-dyes demonstrate good fluorogenic properties, as the free molecules are practically nonfluorescent, while the protein-conjugated forms readily emit light [147,148].

In general, to maximize SNR the dye with suitable fluorescence properties should be chosen in such a way that laser excitation produces strong dye fluorescence in spectral range, where Raman scattering and background luminescence are minimal. For example, after further improvement of photostability and fluorescence quantum yield for the various "red" dyes, this class may become viable for SMD as the efficiencies of both Rayleigh and Raman scattering are greatly diminished by shifting from blue to red excitation, because intensity of scattered light scales with $(\lambda_{ex})^{-4}$ [80,149]. For example, scattering intensity drops three times while going from 488 nm to 640 nm. Moreover, the number of luminescent impurities, which absorb in red and NIR regions, is substantially smaller than molecules which absorb in UV and blue-green regions [108,150]. As a result, fluorescence of native fluorophores emitting in UV are not suitable for highly-sensitive CE-LIF, because of both increased scattering and higher background autofluorescence.

Simultaneous or sequential absorption of two photons and the following emission of light with shorter wavelength may be employed to avoid the impact of Rayleigh and Raman scattering. Nevertheless, the overall properties (absorption cross-section, fluorescence quantum yield, and photostability) of effective two-photon-absorbing organic dyes are still worse than characteristics of typical CE-LIF labels [151]. Also the need for high power density, for simultaneous absorption of two photons, implies the use of special femtosecond lasers and extremely focused (up-to diffraction limit) beams, which may result in very fast photobleaching of fluorescent labels [109], and/or cause physical damage to the capillary. The second option, sequential absorption of two photons, is readily realized only in sophisticated nanoparticle-based dyes [152]. However, their size (mass) is much larger than that of typical labels, and nanoparticles will minimize differences in electrophoretic mobilities of the studied molecules which are essential for efficient separation of multiple analytes. Moreover, it is very difficult to synthesize nanoparticles with a narrow distribution of their charge-to-size ratios that would lead to consistent CE results.

The contaminants present in the BGE or introduced into the sample solution during sample treatment procedures may result in strong autofluorescence background signal in CE-LIF. Therefore, in both BGE and sample preparation we should use as pure/stable solvents/reagents as possible. Even minor traces of impurities may lead to substantial worsening of LOD [58]. Additional purification, such as with Millipore filtration units, does not require expensive or time-consuming procedures [58]. In some cases, BGE irradiation before preparation of sample solution can be applied, leading to a significant decrease in background [95].

8. Conclusion and prospective

In this tutorial, we consider a set of steps to improve LOD along with their efficacy and complexity of implementation. These steps are applicable to on-capillary CE-LIF instruments, both commercial and custom-mode. Though, some of these single steps may result in only a moderate improvement in LOD, their combined use may help to improve detectability significantly, as in the saying "Many a little makes a mickle". The use of pure electrophoretic solvents, directed photodamage of fluorescent contaminants in buffer solutions, and pre-filtration of sample solution are cost-effective, straightforward and fast physico-chemical ways of decreasing the optical background. Digital filtering of the acquired electrophoretic signal can result in overall improvement of SNR, while being simple and inexpensive. A proper beam profile, which fills the capillary hollow, can provide efficient excitation of all analyte molecules passing through the detector. Low-aberration optics is needed to accurately collect fluorescence from the confined space inside the capillary core and minimize background signal for further spatial filtering. For this purpose, *in silico* simulation of the propagation of rays through an optical system may help to choose proper lenses and save time and efforts (Section 4.3).

Transition from regular to high-NA objective lenses is expensive, while providing substantial enhancement in fluorescence light collection. With similar costs, further increase in SNR is achieved by selection of more efficient spatial and spectral filters (Sections 5.1–5.2). In CE-LIF detection, SNR is comparable for analog and photon-counting modes (Section 6.5), thus this parameter should be secondary when choosing a suitable detector. Additional gain in SNR may be obtained with the use of more powerful lasers (Chapters 3–4), which are typically expensive. Before such investments, it is necessary to estimate the possible power increment imposed by photostability of the used fluorophores and utilized optical components. Lifetime filtering provides some increase in SNR, but together with efficient spectral and spatial filtering it results in relatively modest improvements (Section 5.3 and Fig. 14). One of the possible reasons of poor lifetime filtration is the presence of fluorescent impurities whose lifetime is comparable with that of the fluorescent analytes. Lifetime filtering requires a pulse laser and a proper electronic controller board to collect kinetic signals, and, in our view, this technique should be considered as a vital option in CE-LIF, when lifetimes can be used to identify different analytes. Polarization filtering is also worth considering when it may provide additional information on the studied analytes, but SNR improvement has not been proved experimentally (Section 5.4). "Red" dyes are a promising class of labeling molecules as both scattering and background fluorescence are greatly reduced by shifting from blue to red excitation. The number of applications of "red" dyes is growing in the field of laser microscopy; therefore, future progress in efficient labels and powerful "red" lasers may successfully contribute to the field of CE-LIF. We anticipate that "red" is a prospective direction to develop CE-LIF methods for efficient and sensitive detection.

When the studied sample is low-concentrated, the resolving power and LOD should be balanced, as a typical short injected plug with the optimal length for resolving two and more analytes may not contain enough copy-numbers of studied molecules to be detected. As a result, all technical improvements to CE-LIF may lead us to the realization of single-molecule quantification, but in the case of short injected plugs we will always be limited by the error in the number of injected molecules due to the statistical nature of such fluctuations [15]. Single-molecule detection techniques are capable of counting single fluorophore molecules; however, the signal from a statistically significant number of single analyte molecules has to be collected (typically about 100 for a reasonable accuracy and precision [150,153]). Therefore, improvements to sensitivity of on-capillary techniques must be done in parallel with the development and application of advanced procedures. For example, while working with injection methods, pre-concentration of dilute solutions may help to gather statistically appropriate quantity of molecules within a plug of relatively small volume [29]. In order to collect a sufficient number of detected events (more than 100), a plug injection could be substituted by continuous-flow analysis of low-concentrated solutions with single-molecule fluorescent detection and subsequent cross-correlation analysis [21]. Grounded on single-molecule mathematics and pre-concentration techniques, new experimental approaches may be created to

extract additional information from low-concentrated solutions of biological molecules.

In this tutorial, we considered universal approaches to improve sensitivity of CE-LIF detection by increasing acquisition of the useful fluorescent signal and by suppressing the unwanted background. Conceptually, the key approaches include: (i) accurate excitation with appropriate capillary design; (ii) detection of the maximum number of fluorescence photons; (iii) efficient optical filtering techniques (*e.g.* in spatial, spectral and time domains). Advances in chemistry of "red" organic dyes and progress in physics of corresponding lasers and detectors will open new possibilities of sensitive operation within the current basic detection principles. Improvements to the on-capillary detection schemes and signal-treatment methods may further expand the quantitative boundaries of CE-LIF.

Acknowledgments

The authors thank the Natural Sciences and Engineering Research Council of Canada for support: NSERC Discovery Grant (CHRP 462341-2014) to S.N.K. and Banting Postdoctoral Fellowship to A.S.S. Grant (CPG 134747) from the Canadian Institutes of Health Research is also acknowledged. The authors thank Dr. Sven Kochmann and Mirzo Kanoatov for reading the manuscript and providing critical comments.

Appendix A. Supplementary data

Supplementary data related to this article can be found at http://dx.doi.org/10.1016/j.aca.2016.06.015.

References

[1] T.M. Olefirowicz, A.G. Ewing, Detection methods in capillary electrophoresis, in: P.D. Grossman, J.C. Colburn (Eds.), Capillary Electrophoresis: Theory & Practice, Academic Press, Inc., San Diego, 1992, pp. 45–85.
[2] C. Scanlan, T. Lapainis, J.V. Sweedler, Light-based detection methods for capillary electrophoresis, in: J.P. Landers (Ed.), Handbook of Capillary and Microchip Electrophoresis and Associated Microtechniques, CRCPress. Taylor & Francis Group, Boca Raton, 2008, pp. 305–334.
[3] E. Gassmann, J.E. Kuo, R.N. Zare, Electrokinetic separation of chiral compounds, Science 230 (1985) 813–814.
[4] M. Kanoatov, V.A. Galievsky, S.M. Krylova, L.T. Cherney, H.K. Jankowski, S.N. Krylov, Using nonequilibrium capillary electrophoresis of equilibrium mixtures (NECEEM) for simultaneous determination of concentration and equilibrium constant, Anal. Chem. 87 (2015) 3099–3106.
[5] E. Pienaar, M. Theron, M. Nelson, H.J. Viljoen, A quantitative model of error accumulation during PCR amplification, Comput. Biol. Chem. 30 (2006) 102–111.
[6] N. Redshaw, T. Wilkes, A. Whale, S. Cowen, J. Huggett, C.A. Foy, A comparison of miRNA isolation and RT-qPCR technologies and their effects on quantification accuracy and repeatability, BioTechniques 54 (2013) 155–164.
[7] P.C. Stomper, M.E. Nava, R.M. Budnick, C.C. Stewart, Specimen mammography-guided fine-needle aspirates of clinically occult benign and malignant lesions. Analysis of cell number and type, Investig. Radiol. 32 (1997) 277–281.
[8] G. Wiedswang, E. Borgen, R. Karesen, B. Naume, Detection of isolated tumor cells in BM from breast-cancer patients: significance of anterior and posterior iliac crest aspirations and the number of mononuclear cells analyzed, Cytotherapy 5 (2003) 40–45.
[9] M.A. Lewandowska, W. Jozwicki, C. Jochymski, J. Kowalewski, Application of PCR methods to evaluate EGFR, KRAS and BRAF mutations in a small number of tumor cells in cytological material from lung cancer patients, Oncol. Rep. 30 (2013) 1045–1052.
[10] M. Mascalchi, M. Falchini, C. Maddau, F. Salvianti, M. Nistri, E. Bertelli, L. Sali, S. Zuccherelli, A. Vella, M. Matucci, L. Voltolini, A.L. Pegna, M. Luconi, P. Pinzani, M. Pazzagli, Prevalence and number of circulating tumour cells and microemboli at diagnosis of advanced NSCLC, J. Cancer Res. Clin. Oncol. 142 (2016) 195–200.
[11] Y. Liang, D. Ridzon, L. Wong, C. Chen, Characterization of microRNA expression profiles in normal human tissues, BMC Genom. 8 (2007) 166.
[12] J. Lu, A. Tsourkas, Imaging individual microRNAs in single mammalian cells in situ, Nucleic Acids Res. 37 (2009) e100.
[13] J.P. Landers, Introduction to capillary electrophoresis, in: J.P. Landers (Ed.), Capillary and Microchip Electrophoresis and Associated Microtechniques, Taylor & Francis Group, LLC, Boca Raton, 2008, pp. 3–74.
[14] D.W. Wegman, L.T. Cherney, G.M. Yousef, S.N. Krylov, Universal drag tag for direct quantitative analysis of multiple microRNAs, Anal. Chem. 85 (2013) 6518–6523.
[15] D.Y. Chen, N.J. Dovichi, Single-molecule detection in capillary electrophoresis: molecular shot noise as a fundamental limit to chemical analysis, Anal. Chem. 68 (1996) 690–696.
[16] M.E. Johnson, J.P. Landers, Fundamentals and practice for ultrasensitive laser-induced fluorescence detection in microanalytical systems, Electrophoresis 25 (2004) 3513–3527.
[17] J.R. Lakowicz, Single-molecule Detection, Principles of Fluorescence Spectroscopy, Springer Science+Business Media, LLC, New York, 2006, pp. 757–795.
[18] W. Becker, H. Hickl, C. Zander, K.H. Drexhage, M. Sauer, S. Siebert, J. Wolfrum, Time-resolved detection and identification of single analyte molecules in microcapillaries by time-correlated single-photon counting (TCSPC), Rev. Sci. Instrum. 70 (1999) 1835–1841.
[19] K. Dörre, J. Stephan, M. Eigen, Highly efficient single molecule detection in different micro and submicrometer channels with cw-excitation, Single Mol. 2 (2001) 165–175.
[20] A. Lundqvist, D.T. Chiu, O. Orwar, Electrophoretic separation and confocal laser-induced fluorescence detection at ultralow concentrations in constricted fused-silica capillaries, Electrophoresis 24 (2003) 1737–1744.
[21] P.G. Schiro, C.L. Kuyper, D.T. Chiu, Continuous-flow single-molecule CE with high detection efficiency, Electrophoresis 28 (2007) 2430–2438.
[22] E.A. Doherty, R.J. Meagher, M.N. Albarghouthi, A.E. Barron, Microchannel wall coatings for protein separations by capillary and chip electrophoresis, Electrophoresis 24 (2003) 34–54.
[23] S. de Jong, S.N. Krylov, Pressure-based approach for the analysis of protein adsorption in capillary electrophoresis, Anal. Chem. 84 (2012) 453–458.
[24] N.J. Dovichi, J.C. Martin, J.H. Jett, R.A. Keller, Attogram detection limit for aqueous dye samples by laser-induced fluorescence, Science 219 (1983) 845–847.
[25] O.O. Dada, B.J. Huge, N.J. Dovichi, Simplified sheath flow cuvette design for ultrasensitive laser induced fluorescence detection in capillary electrophoresis, Analyst 137 (2012) 3099–3101.
[26] Y.F. Cheng, N.J. Dovichi, Subattomole amino acid analysis by capillary zone electrophoresis and laser-induced fluorescence, Science 242 (1988) 562–564.
[27] D.Y. Chen, K. Adelhelm, X.L. Cheng, N.J. Dovichi, Communication. A simple laser-induced fluorescence detector for sulforhodamine 101 in a capillary electrophoresis system: detection limits of 10 yoctomoles or six molecules, Analyst 119 (1994) 349.
[28] O.O. Dada, D.C. Essaka, O. Hindsgaul, M.M. Palcic, J. Prendergast, R.L. Schnaar, N.J. Dovichi, Nine orders of magnitude dynamic range: picomolar to millimolar concentration measurement in capillary electrophoresis with laser induced fluorescence detection employing cascaded avalanche photodiode photon counters, Anal. Chem. 83 (2011) 2748–2753.
[29] D.W. Wegman, F. Ghasemi, A. Khorshidi, B.B. Yang, S.K. Liu, G.M. Yousef, S.N. Krylov, Highly-sensitive amplification-free analysis of multiple miRNAs by capillary electrophoresis, Anal. Chem. 87 (2015) 1404–1410.
[30] B.B. Haab, R.A. Mathies, Single molecule fluorescence burst detection of DNA fragments separated by capillary electrophoresis, Anal. Chem. 67 (1995) 3253–3260.
[31] F. Zarrin, N.J. Dovichi, Sub-picoliter detection with the sheath flow cuvette, Anal. Chem. 57 (1985) 2690–2692.
[32] A.T. Timperman, K. Khatib, J.V. Sweedler, Wavelength-resolved fluorescence detection in capillary electrophoresis, Anal. Chem. 67 (1995) 139–144.
[33] A. Castro, E.B. Shera, Single-Molecule electrophoresis, Anal. Chem. 67 (1995) 3181–3186.
[34] M. Sauer, J. Hofkens, J. Enderlein, Fluorophores and Fluorescent Labels, Handbook of Fluorescence Spectroscopy and Imaging, WILEY-VCH Verlag & Co. KGaA, Weinheim, Germany, 2011, pp. 31–60.
[35] N.J. Dovichi, J.C. Martin, J.H. Jett, M. Trkula, R.A. Keller, Laser-induced fluorescence of flowing samples as an approach to single-molecule detection in liquids, Anal. Chem. 56 (1984) 348–354.
[36] S. Wu, N.J. Dovichi, High-sensitivity fluorescence detector fluorescein isothiocyanate derivatives of amino acids separated by capillary zone electrophoresis, J. Chromatogr. 480 (1989) 141–155.
[37] T. Erdogan, Optical filters for wavelength selection in fluorescence instrumentation, Current protocols in cytometry 56 (2011) 2.4.1–2.4.25.
[38] M.D. Eisaman, J. Fan, A. Migdall, S.V. Polyakov, Invited review article: single-photon sources and detectors, Rev. Sci. Instrum. 82 (2011) 071101.
[39] https://www.picoquant.com/products/category/picosecond-pulsed-sources/ldh-series-picosecond-pulsed-diode-laser-heads#custom2 and http://www.becker-hickl.com/lasers.htm (Date of access: June 01, 2016).
[40] A. Gulinatti, N. Bertone, Single-photon detectors: planar architecture optimizes Si single-photon-counting detectors, Laser Focus World (November 2011) 49–53.
[41] Z.X. Zhang, F. Zhang, Y. Liu, Recent advances in enhancing the sensitivity and resolution of capillary electrophoresis, J. Chromatogr. Sci. 51 (2013) 666–683.
[42] F. Kitagawa, K. Otsuka, Recent applications of on-line sample preconcentration techniques in capillary electrophoresis, J. Chromatogr. A 1335 (2014) 43–60.

[43] M. Hink, Single-molecule microscopy using silicone oil immersion objective lenses, Biomed. Sci. 56 (2012) 83–85.
[44] B.J. Dodgson, S.N. Krylov, Time-resolved detection of luminescence for electrophoretic methods, Trac-Trend Anal. Chem. 33 (2012) 23–34.
[45] C. Dong, J. Ren, Coupling of fluorescence correlation spectroscopy with capillary and microchannel analytical systems and its applications, Electrophoresis 35 (2014) 2267–2278.
[46] R. Stewart, I. Gideoni, Y. Zhu, Signal processing methods for capillary electrophoresis, in: N.-S. Yang (Ed.), Systems and Computational Biology - Bioinformatics and Computational Modeling, InTech, 2011, pp. 311–334. Available from: http://www.intechopen.com/books/systems-and-computational-biology-bioinformatics-and-computationalmodeling/signal-processing-methods-for-capillary-electrophoresis.
[47] M. Szumski, B. Buszewski, Qualitative and quantitative analysis: interpretation of electropherograms, in: B. Buszewski, E. Dziubakiewicz, M. Szumski (Eds.), Electromigration Techniques. Theory and Practice, Springer, Heidelberg, 2013, pp. 69–75.
[48] P.S. Dittrich, A. Manz, Single-molecule fluorescence detection in microfluidic channels–the Holy Grail in muTAS? Anal. Bioanal. Chem. 382 (2005) 1771–1782.
[49] M. Bohmer, J. Enderlein, Fluorescence spectroscopy of single molecules under ambient conditions: methodology and technology, ChemPhysChem 4 (2003) 793–808.
[50] J. Enderlein, D.L. Robbins, W.P. Ambrose, P.M. Goodwin, R.A. Keller, Statistics of single-molecule detection, J. Phys. Chem. B 101 (1997) 3626–3632.
[51] M. Sauer, J. Hofkens, J. Enderlein, Fluorescence Correlation Spectroscopy, Handbook of Fluorescence Spectroscopy and Imaging: from Ensemble to Single Molecules, WILEY-VCH Verlag & Co. KGaA, Weinheim, Germany, 2011, pp. 93–146.
[52] M. Thompson, S.L.R. Ellison, R. Wood, Harmonized guidelines for single-laboratory validation of methods of analysis - (IUPAC technical report), Pure Appl. Chem. 74 (2002) 835–855.
[53] Validation of Analytical Procedures: Text and Methodology Q2(R1), ICH Harmonised Tripartite Guideline, 2005.
[54] J.E. Knoll, Estimation of the limit of detection in chromatography, J. Chromatogr. Sci. 23 (1985) 422–425.
[55] H. Nasim, Y. Jamil, Diode lasers: from laboratory to industry, Opt. Laser Technol. 56 (2014) 211–222.
[56] E. Ban, E.J. Song, Recent developments and applications of capillary electrophoresis with laser-induced fluorescence detection in biological samples, J. Chromatogr. B Anal. Technol. Biomed. Life Sci. 929 (2013) 180–186.
[57] R.Y. Tsien, L. Ernst, A. Waggoner, Fluorophores for confocal microscopy: photophysics and photochemistry, in: James B. Pawley (Ed.), Handbook of Biological Confocal Microscopy, Springer Science+Business Media, LLC, New York, 2006, pp. 338–352.
[58] F. Ghasemi, D.W. Wegman, M. Kanoatov, B.B. Yang, S.K. Liu, G.M. Yousef, S.N. Krylov, Improvements to direct quantitative analysis of multiple microRNAs facilitating faster analysis, Anal. Chem. 85 (2013) 10062–10066.
[59] B.J. Dodgson, A. Mazouchi, D.W. Wegman, C.C. Gradinaru, S.N. Krylov, Detection of a thousand copies of miRNA without enrichment or modification, Anal. Chem. 84 (2012) 5470–5474.
[60] T. Hirschfeld, Quantum efficiency independence of the time integrated emission from a fluorescent molecule, Appl. Opt. 15 (1976) 3135–3139.
[61] A. Diaspro, G. Chirico, C. Usai, P. Ramoino, J. Dobrucki, Photobleaching, in: J.B. Pawley (Ed.), Handbook of Biological Confocal Microscopy, Springer Science+Business Media, LLC, New York, 2006, pp. 690–702.
[62] R. Sjoback, J. Nygren, M. Kubista, Absorption and fluorescence properties of fluorescein, Spectrochim. Acta A 51 (1995) L7–L21.
[63] B. Soep, M. Martin, A. Kellmann, L. Lindqvis, Study of triplet quantum yields using a tunable dye laser, Chem. Phys. Lett. 13 (1972) 241–244.
[64] A. Mazouchi, B.J. Dodgson, D.W. Wegman, S.N. Krylov, C.C. Gradinaru, Ultrasensitive on-column laser-induced fluorescence in capillary electrophoresis using multiparameter confocal detection, Analyst 137 (2012) 5538–5545.
[65] Y. Xu, S. Chen, X. Feng, W. Du, Q. Luo, B.F. Liu, On-column detection of multiphoton-excited fluorescence in CE using hyphenated cylindrical-square capillaries, Electrophoresis 29 (2008) 734–739.
[66] Y. Fujimoto, D. Nishiwaki, Objective Lens System for Microscope, Patent US 6,747,804 B2, Olympus Corporation, 2004.
[67] H. Konishi, Y. Fujimoto, K. Kusaka, T. Kasahara, Immersion Type Microscope Objective, Patent US 7,486,445 B2, Olympus Corporation, 2009.
[68] M.T. Veledo, P. Lara-Quintanar, M. de Frutos, J.C. Díez-Masa, Fluorescence detection in capillary electrophoresis, in: M.L. Marina, A. Rios, M. Valcarcel (Eds.), Comprehensive Analytical Chemistry (Analysis and Detection by Capillary Electrophoresis), Elsevier Science, 2005, pp. 305–374.
[69] W. Becker, Advanced Time-Correlated Single Photon Counting Techniques, Springer, Berlin Heidelberg, 2005.
[70] M. Macka, T. Piasecki, P.K. Dasgupta, Light-emitting diodes for analytical chemistry, Annu. Rev. Anal. Chem. 7 (2014) 183–207.
[71] F. Huo, H. Yuan, X. Yang, M.C. Breadmore, D. Xiao, Pulsed multi-wavelength excitation using fiber-in-capillary light emitting diode induced fluorescence detection in capillary electrophoresis, Talanta 83 (2010) 521–526.
[72] F. Huo, R. Guijt, D. Xiao, M.C. Breadmore, Dual wavelength excitation fluorescence detector for capillary electrophoresis using a pulsed bi-colour light emitting diode, Analyst 136 (2011) 2234–2241.
[73] H. Ji, M. Li, L. Guo, H. Yuan, C. Wang, D. Xiao, Design and evaluation of capillary coupled with optical fiber light-emitting diode induced fluorescence detection for capillary electrophoresis, Electrophoresis 34 (2013) 2546–2552.
[74] J. Huhner, A. Ingles-Prieto, C. Neususs, M. Lammerhofer, H. Janovjak, Quantification of riboflavin, flavin mononucleotide, and flavin adenine dinucleotide in mammalian model cells by CE with LED-induced fluorescence detection, Electrophoresis 36 (2015) 518–525.
[75] J. Enzonga, V. Ong-Meang, F. Couderc, A. Boutonnet, V. Poinsot, M.M. Tsieri, T. Silou, J. Bouajila, Determination of free amino acids in African gourd seed milks by capillary electrophoresis with light-emitting diode induced fluorescence and laser-induced fluorescence detection, Electrophoresis 34 (2013) 2632–2638.
[76] https://www.thorlabs.com/newgrouppage9.cfm?objectgroup_id=2692 (Date of access: June 01, 2016).
[77] https://www.newport.com/laser-diode-technology (Date of access: June 01, 2016).
[78] https://www.thorlabs.com/newgrouppage9.cfm?objectgroup_id=5206 (Date of access: June 01, 2016).
[79] H.E. Keller, Objective lenses for confocal microscopy, in: J.B. Pawley (Ed.), Handbook of Biological Confocal Microscopy, Springer Science+Business Media, LLC, New York, 2006, pp. 145–161.
[80] V. Buschmann, K.D. Weston, M. Sauer, Spectroscopic study and evaluation of red-absorbing fluorescent dyes, Bioconj. Chem. 14 (2003) 195–204.
[81] W. Becker, The bh TCSPC Handbook, sixth ed., Becker & Hickl GmbH, Berlin, 2015. Available from: http://www.becker-hickl.com.
[82] Q. Li, S. Seeger, Autofluorescence detection in analytical chemistry and biochemistry, Appl. Spectrosc. Rev. 45 (2010) 12–43.
[83] B.J. de Kort, G.J. de Jong, G.W. Somsen, Native fluorescence detection of biomolecular and pharmaceutical compounds in capillary electrophoresis: detector designs, performance and applications: a review, Anal. Chim. acta 766 (2013) 13–33.
[84] L. Hernandez, J. Escalona, N. Joshi, N. Guzman, Laser-induced fluorescence and fluorescence microscopy for capillary electrophoresis zone detection, J. Chromatogr. 559 (1991) 183–196.
[85] R.H. Webb, Confocal optical microscopy, Rep. Prog. Phys. 59 (1996) 427.
[86] T.R. Corle, G.S. Kino, Depth, Transverse Resolution, Confocal Scanning Optical Microscopy and Related Imaging Systems, Academic Press, Inc, 1996, pp. 147–223.
[87] Y. Zhu, N. Chen, Q. Li, Q. Fang, Improving the sensitivity of confocal laser induced fluorescence detection to the sub-picomolar scale for round capillaries by laterally shifting the laser focus point, Analyst 138 (2013) 4642–4648.
[88] P.K. Narayanaswamy, The Raman spectra of water, heavy water and ice, Proc. Indian Acad. Sci. – Sect. A 27 (1948) 311–315.
[89] G.E. Walrafen, Raman spectral studies of water structure, J. Chem. Phys. 40 (1964) 3249–3256.
[90] R.H. Stolen, G.E. Walrafen, Water and its relation to broken bond defects in fused silica, J. Chem. Phys. 64 (1976) 2623–2631.
[91] P.F. Mcmillan, R.L. Remmele, Hydroxyl sites in SiO_2 glass - a note on infrared and Raman-spectra, Am. Mineral. 71 (1986) 772–778.
[92] M. Tanaka, R.J. Young, Review Polarised Raman spectroscopy for the study of molecular orientation distributions in polymers, J. Mater. Sci. 41 (2006) 963–991.
[93] Y. Tominaga, A. Fujiwara, Y. Amo, Dynamical structure of water by Raman spectroscopy, Fluid Phase Equilib. 144 (1998) 323–330.
[94] P. Mcmillan, B. Piriou, Raman-spectroscopic studies of silicate and related glass structure - a review, B Mineral. 106 (1983) 57–75.
[95] L.M. Ramsay, J.A. Dickerson, O. Dada, N.J. Dovichi, Femtomolar concentration detection limit and zeptomole mass detection limit for protein separation by capillary isoelectric focusing and laser-induced fluorescence detection, Anal. Chem. 81 (2009) 1741–1746.
[96] D.C. Essaka, J. Prendergast, R.B. Keithley, M.M. Palcic, O. Hindsgaul, R.L. Schnaar, N.J. Dovichi, Metabolic cytometry: capillary electrophoresis with two-color fluorescence detection for the simultaneous study of two glycosphingolipid metabolic pathways in single primary neurons, Anal. Chem. 84 (2012) 2799–2804.
[97] E. Ban, D.K. Chae, E.J. Song, Simultaneous detection of multiple microRNAs for expression profiles of microRNAs in lung cancer cell lines by capillary electrophoresis with dual laser-induced fluorescence, J. Chromatogr. A 1315 (2013) 195–199.
[98] W. Becker, Advanced Time-correlated Single Photon Counting Techniques, Springer, Berlin Heidelberg, 2005.
[99] http://www.micro-photon-devices.com/Products/Photon-Counters (Date of access: June 01, 2016).
[100] http://www.idquantique.com/photon-counting/photon-counting-modules/ (Date of access: June 01, 2016).
[101] http://www.lasercomponents.com/us/product/single-photon-counting-modules/(Date of access: June 01, 2016).
[102] Y. Yamaguchi, K. Hashino, M. Ito, K. Ikawa, T. Nishioka, K. Matsumoto, Sodium dodecyl sulfate polyacrylamide slab gel electrophoresis and hydroxyethyl cellurose gel capillary electrophoresis of luminescent lanthanide chelate-labeled proteins with time-resolved detection, Anal. Sci. Int. J. Jpn. Soc. Anal. Chem. 25 (2009) 327–332.
[103] I. Lammers, J. Buijs, F. Ariese, C. Gooijer, Sensitized enantioselective laser-

induced phosphorescence detection in chiral capillary electrophoresis, Anal. Chem. 82 (2010) 9410–9417.
[104] M. Castro-Puyana, I. Lammers, J. Buijs, C. Gooijer, F. Ariese, Quenched phosphorescence as alternative detection mode in the chiral separation of methotrexate by electrokinetic chromatography, Anal. Bioanal. Chem. 400 (2011) 2913–2919.
[105] A.A. Istratov, O.F. Vyvenko, Exponential analysis in physical phenomena, Rev. Sci. Instrum. 70 (1999) 1233.
[106] S.D. Llopis, W. Stryjewski, S.A. Soper, Near-infrared time-resolved fluorescence lifetime determinations in poly(methylmethacrylate) microchip electrophoresis devices, Electrophoresis 25 (2004) 3810–3819.
[107] T.M. Snyder, L.B. McGown, Multiplex single strand conformation polymorphism analysis by capillary electrophoresis with on-the-fly fluorescence lifetime detection, Appl. Spectrosc. 59 (2005) 335–339.
[108] S. McWhorter, S.A. Soper, Near-infrared laser-induced fluorescence detection in capillary electrophoresis, Electrophoresis 21 (2000) 1267–1280.
[109] C. Eggeling, A. Volkmer, C.A. Seidel, Molecular photobleaching kinetics of Rhodamine 6G by one- and two-photon induced confocal fluorescence microscopy, ChemPhysChem 6 (2005) 791–804.
[110] C. Eggeling, J. Widengren, L. Brand, J. Schaffer, S. Felekyan, C.A. Seidel, Analysis of photobleaching in single-molecule multicolor excitation and Forster resonance energy transfer measurements, J. Phys. Chem. A 110 (2006) 2979–2995.
[111] P. Schulze, M. Ludwig, D. Belder, Impact of laser excitation intensity on deep UV fluorescence detection in microchip electrophoresis, Electrophoresis 29 (2008) 4894–4899.
[112] J.A. Smyder, A.R. Amori, M.Y. Odoi, H.A. Stern, J.J. Peterson, T.D. Krauss, The influence of continuous vs. pulsed laser excitation on single quantum dot photophysics, Phys. Chem. Chem. Phys. PCCP 16 (2014) 25723–25728.
[113] J.R. Lakowicz, Fluorescence Anisotropy, Principles of Fluorescence Spectroscopy, Springer Science+Business Media, LLC, New York, 2006, pp. 353–382.
[114] M. Koshioka, K. Sasaki, H. Masuhara, Time-dependent fluorescence depolarization analysis in three-dimensional microspectroscopy, Appl. Spectrosc. 49 (1995) 224–228.
[115] J. Enderlein, Theoretical investigation of aspects of single-molecule fluorescence detection in microcapillaries, Cytometry 36 (1999) 195–199.
[116] J.C. Fister, S.C. Jacobson, J.M. Ramsey, Ultrasensitive cross correlation electrophoresis on microchip devices, Anal. Chem. 71 (1999) 4460–4464.
[117] H.J. Crabtree, M.U. Kopp, A. Manz, Shah convolution fourier transform detection, Anal. Chem. 71 (1999) 2130–2138.
[118] J.D. Inge, S.R. Crouch, Optical Sources, Transducers, and Measurement Systems, Spectrochemical Analysis, Prentice-Hall, Inc., New Jersey, 1988, pp. 87–134.
[119] H.D. Luke, The origins of the sampling theorem, Ieee Commun. Mag. 37 (1999) 106–108.
[120] P.S.R. Diniz, E.A.B. da Silva, S.L. Netto, Digital Signal Processing: System Analysis and Design, Cambridge University Press, 2002.
[121] H.H. Madden, Comments on the Savitzky-Golay convolution method for least-squares-fit smoothing and differentiation of digital data, Anal. Chem. 50 (1978) 1383–1386.
[122] D.Y. Chen, N.J. Dovichi, Yoctomole detection limit by laser-induced fluorescence in capillary electrophoresis, J. Chromatogr. B Biomed. Appl. 657 (1994) 265–269.
[123] T. Kaneta, Transformation techniques for capillary and microchip electrophoresis, in: G. Hanrahan, F.A. Gomez (Eds.), Chemometric Methods in Capillary Electrophoresis, John Wiley & Sons, 2010, pp. 391–406.
[124] B.F. Liu, Y. Sera, N. Matsubara, K. Otsuka, S. Terabe, Signal denoising and baseline correction by discrete wavelet transform for microchip capillary electrophoresis, Electrophoresis 24 (2003) 3260–3265.
[125] Q.W. Gao, Y.X. Lu, D. Sun, D.X. Zhang, A multiscale products technique for denoising of DNA capillary electrophoresis signals, Meas. Sci. Technol. 24 (2013) 065004.
[126] M. Li, H. Ji, J. Li, H. Yuan, D. Xiao, A high-sensitivity LIF detector with silver mirror coating detection window and small-angle optical deflection from collinear system for CE, Electrophoresis 34 (2013) 3163–3170.
[127] C. Huhn, L.R. Ruhaak, J. Mannhardt, M. Wuhrer, C. Neususs, A.M. Deelder, H. Meyer, Alignment of laser-induced fluorescence and mass spectrometric detection traces using electrophoretic mobility scaling in CE-LIF-MS of labeled N-glycans, Electrophoresis 33 (2012) 563–566.
[128] K. Kamagata, T. Kawaguchi, Y. Iwahashi, A. Baba, K. Fujimoto, T. Komatsuzaki, Y. Sambongi, Y. Goto, S. Takahashi, Long-term observation of fluorescence of free single molecules to explore protein-folding energy landscapes, J. Am. Chem. Soc. 134 (2012) 11525–11532.
[129] G. Nouadje, M. Nertz, P. Verdeguer, F. Couderc, Ball-lens laser-induced fluorescence detector as an easy-to-use highly sensitive detector for capillary electrophoresis - application to the identification of biogenic-amines in dairy-products, J. Chromatogr. A 717 (1995) 335–343.
[130] A. Rodat, F. Kalck, V. Poinsot, B. Feurer, F. Couderc, An ellipsoidal mirror for detection of laser-induced fluorescence in capillary electrophoresis system: applications for labelled antibody analysis, Electrophoresis 29 (2008) 740–746.
[131] V. Amirkhanian, S.S. Deliwala, R.W. Franck, B.J. Wanders, G. Tepermeister, Miniature multiple wavelength excitation and emission optical system and method for laser-induced fluorescence detectors in capillary electrophoresis, Patent US 6,184,990 B1, Beckman Coulter, Inc., 2001.
[132] Hamamatsu Photonics, Photomultiplier Tubes. Basics and applications, Hamamatsu Photonics K.K, 2007. Available from: http://www.hamamatsu.com/resources/pdf/etd/PMT_handbook_v3aE.pdf.
[133] C.D. Whitmore, D. Essaka, N.J. Dovichi, Six orders of magnitude dynamic range in capillary electrophoresis with ultrasensitive laser-induced fluorescence detection, Talanta 80 (2009) 744–748.
[134] http://www.emccd.com/(Date of access: June 01, 2016).
[135] X. Zhang, J.N. Stuart, J.V. Sweedler, Capillary electrophoresis with wavelength-resolved laser-induced fluorescence detection, Anal. Bioanal. Chem. 373 (2002) 332–343.
[136] J.D. Inge, S.R. Crouch, Signal-to-Noise Ratio Considerations, Spectrochemical Analysis, Prentice-Hall, Inc., New Jersey, 1988, pp. 135–163.
[137] J.R. Lakowicz, Instrumentation for Fluorescence Spectroscopy, Principles of Fluorescence Spectroscopy, Springer Science+Business Media, LLC, New York, 2006, pp. 27–61.
[138] W.J. Underberg, J.C. Waterval, Derivatization trends in capillary electrophoresis: an update, Electrophoresis 23 (2002) 3922–3933.
[139] Z. Glatz, On-capillary derivatisation as an approach to enhancing sensitivity in capillary electrophoresis, Electrophoresis 36 (2015) 744–763.
[140] A. Wuethrich, J.P. Quirino, Derivatisation for separation and detection in capillary electrophoresis (2012-2015), Electrophoresis 37 (2016) 45–55.
[141] D.W. Wegman, S.N. Krylov, Direct quantitative analysis of multiple miRNAs (DQAMmiR), Angew. Chem. 50 (2011) 10335–10339.
[142] D.W. Wegman, F. Ghasemi, A.S. Stasheuski, A. Khorshidi, B.B. Yang, S.K. Liu, G.M. Yousef, S.N. Krylov, Achieving single-nucleotide specificity in direct quantitative analysis of multiple MicroRNAs (DQAMmiR), Anal. Chem. 88 (2016) 2472–2477.
[143] M.S. Goncalves, Fluorescent labeling of biomolecules with organic probes, Chem. Rev. 109 (2009) 190–212.
[144] N. Panchuk-Voloshina, R.P. Haugland, J. Bishop-Stewart, M.K. Bhalgat, P.J. Millard, F. Mao, W.Y. Leung, R.P. Haugland, Alexa dyes, a series of new fluorescent dyes that yield exceptionally bright, photostable conjugates, J. Histochem Cytochem 47 (1999) 1179–1188.
[145] M. Heilemann, S. van de Linde, A. Mukherjee, M. Sauer, Super-resolution imaging with small organic fluorophores, Angew. Chem. 48 (2009) 6903–6908.
[146] B.K. Wetzl, S.M. Yarmoluk, D.B. Craig, O.S. Wolfbeis, Chameleon labels for staining and quantifying proteins, Angew. Chem. 43 (2004) 5400–5402.
[147] K.E. Swearingen, J.A. Dickerson, E.H. Turner, L.M. Ramsay, R. Wojcik, N.J. Dovichi, Reaction of fluorogenic reagents with proteins II: capillary electrophoresis and laser-induced fluorescence properties of proteins labeled with Chromeo P465, J. Chromatogr. A 1194 (2008) 249–252.
[148] E.H. Turner, J.A. Dickerson, L.M. Ramsay, K.E. Swearingen, R. Wojcik, N.J. Dovichi, Reaction of fluorogenic reagents with proteins III. Spectroscopic and electrophoretic behavior of proteins labeled with Chromeo P503, J. Chromatogr. A 1194 (2008) 253–256.
[149] K. Kolmakov, V.N. Belov, J. Bierwagen, C. Ringemann, V. Muller, C. Eggeling, S.W. Hell, Red-emitting rhodamine dyes for fluorescence microscopy and nanoscopy, Chemistry 16 (2010) 158–166.
[150] S.A. Soper, B.L. Legendre, Single-molecule detection in the near-IR using continuous-wave diode laser excitation with an avalanche photon detector, Appl. Spectrosc. 52 (1998) 1–6.
[151] M. Pawlicki, H.A. Collins, R.G. Denning, H.L. Anderson, Two-photon absorption and the design of two-photon dyes, Angew. Chem. 48 (2009) 3244–3266.
[152] D.E. Achatz, R. Ali, O.S. Wolfbeis, Luminescent chemical sensing, biosensing, and screening using upconverting nanoparticles, Top. Curr. Chem. 300 (2011) 29–50.
[153] J. Enderlein, P.M. Goodwin, A. VanOrden, W.P. Ambrose, R. Erdmann, R.A. Keller, A maximum likelihood estimator to distinguish single molecules by their fluorescence decays, Chem. Phys. Lett. 270 (1997) 464–470.

Prof. Sergey N. Krylov obtained his M.Sc. degree in Physics in 1987 and Ph.D. degree in Biophysical Chemistry in 1990, both from Lomonosov Moscow State University. His postdoctoral training was with Prof. H. Brian Dunford and Prof. Norman J. Dovichi at the University of Alberta. In year 2000, he accepted a position of Associate Professor in the Department of Chemistry at York University in Toronto, where he was promoted to Professor in 2006. In 2003–2013, he held Canada Research Chair Tier II in Bioanalytical Chemistry. In 2015 he was appointed York Research Chair Tier I. He is a founder and Inaugural Director of the Centre for Research on Biomolecular Interactions at York University. He is recognized internationally for his pioneering work in the fields of chemical cytometry, kinetic analysis of affinity interactions, and methods for selection and applications of oligonucleotide aptamers. He recently became interested in development of innovative technologies for cancer subtyping and continuous-flow small-scale chemical manufacturing. His research contributions have been recognized with a number of awards including Petro Canada Young Investigator Award, Premier's Research

Excellence Award, President's Research Excellence Award (York University) and two recognitions from the Chemical Society of Canada: McBryde Medal and Maxxam Award.

Victor A. Galievsky after graduation the Belarusian State University worked at the Institute of Molecular and Atomic Physics of the National Academy of Sciences of Belarus, where obtained his Ph.D. degree in Physics and Mathematics in 2000. He continued his research at the B.I. Stepanov Institute of Physics (Minsk, Belarus), the Institute of Physical Chemistry (Warsaw, Poland) and the Max-Planck-Institute for Biophysical Chemistry (Göttingen, Germany). Since 2011 he has been working as Research Associate in Prof. Krylov's group at York University. He is the author of over 50 peer-reviewed papers. His current research focuses on the development of advanced laser instrumentation for kinetic analysis of affinity interactions.

Alexander S. Stasheuski obtained his Ph.D. degree in Physics and Mathematics at the B.I. Stepanov Institute of Physics of the National Academy of Sciences of Belarus in 2013. He was awarded the Banting Postdoctoral Fellowship and joined Prof. Krylov's group at York University in 2014. He is the coauthor of 18 peer reviewed papers. His current scientific research involves development of a highly sensitive technique for identification of cancer subtypes through the quantitative analysis of microRNA signatures.